

0.5 eV QCD Axion Dark Matter

Noah Bray-Ali

Science Synergy
Los Angeles, CA 90045, USA
E-mail: nbrayali@gmail.com

Abstract. A solution to the dark matter problem of astroparticle physics is presented in the context of an expanding universe cosmology. The solution includes an explicit model for the particle nature of 0.5 eV quantum chromodynamic (QCD) axion dark matter. A direct experimental determination of the QCD axion dark matter rest-mass energy to 44 parts per million precision is given and a cosmological argument is made that QCD axions with this rest-mass energy form the dark matter in the universe.

Contents

1	Introduction	1
2	0.5 eV QCD Axion Dark Matter Model	3
2.1	Chirality and Helicity: What's the Difference?	3
2.2	Continuous $U(1)_A$ Axial Phase Symmetry	4
2.3	Discrete Space-Time Symmetries: \mathcal{P} , \mathcal{C} , \mathcal{T} and All That	5
2.4	0.5 eV QCD Axion Dark Matter at Last	5
2.5	An Instanton Comment on 0.5 eV QCD Axion Dark Matter	6
2.6	Summary: There are Twelve Flavors of 0.5 eV QCD Axion Dark Matter	7
3	0.5 eV QCD Axion Dark Matter Rest-Mass Energy Prediction	7
3.1	Massless Mirror Matter Confined within 0.5 eV QCD Axion Dark Matter	8
3.2	Big Bang Temperature from QCD Axion Angle Jump $\Delta\theta_A = \pi$	9
3.3	0.5 eV QCD Axion Dark Matter Rest-Mass Energy Prediction at Last	10
3.4	Comment on Axion-Photon Coupling of 0.5 eV QCD Axion Dark Matter	11
3.5	Summary of 0.5 eV QCD Axion Rest-Mass Energy Prediction	12
4	0.5 eV QCD Axion Dark Matter Rest-Mass Energy Determination	12
4.1	Principle of 0.5 eV QCD Axion Dark Matter Photoproduction	12
4.2	0.5 eV QCD Axion Dark Matter Photoproduction Experimental Details	13
4.3	0.5 eV QCD Axion Dark Matter Rest-Mass Energy to 44 ppm At Last	14
4.4	Confirmation of 0.5 eV QCD Axion Dark Matter Axion-Photon Coupling Strength	16
4.5	Summary of 0.5 eV QCD Axion Dark Matter Rest-Mass Determination	17
5	0.5 eV QCD Axion Dark Matter Implications	17
5.1	0.5 eV QCD Axion Dark Matter Shifts α	18
5.2	0.5 eV QCD Axion Dark Matter Shifts α_s	19
5.3	0.5 eV QCD Axion Dark Matter Shifts $a_\mu^{\pi\pi}$	22
5.4	Comment on 0.5 eV QCD Axion Dark Matter Local Energy Density	25
5.5	Summary of 0.5 eV QCD Axion Dark Matter Implications	26
6	Conclusion	27
6.1	How Cold is 0.5 eV QCD Axion Dark Matter?	28
6.2	How Does 0.5 eV QCD Axion Dark Matter Effect Big Bang Nucleosynthesis?	29
6.3	How Does 0.5 eV QCD Axion Dark Matter Mess with Stars?	30
6.4	Comment on White Dwarfs, Red Giants, Pulsars, and Supernova 1987A	31
6.5	Summary of 0.5 eV QCD Axion Dark Matter Conclusions	32

1 Introduction

The concept of dark matter in cosmology emerged in the early 1930s in response to the observational evidence for the expansion of the universe [1]. The roughly linear increase in the spectroscopic redshift of spiral galaxies with increasing distance had been argued to be a cosmological effect of an expanding universe sometime earlier [2]. But a large scatter was

reported in the redshift of galaxies in the Coma cluster [3]. Follow-up studies of both the Coma cluster [4] and Virgo cluster [5] soon confirmed that the large spread in redshift within a cluster could be understood in terms of a corresponding spread in the radial velocities of galaxies caused by the gravitation of a large amount of dark matter.

By the end of the 1930s, observations of the nearby Andromeda galaxy M31 [6] and the large apparent diameter elliptical galaxy NGC 3115 [7] found *flat* rotation curves $v(r) \sim \text{const.}$ These observations were contrasted — *at the time* — with the $v(r) \sim 1/\sqrt{r}$ fall-off of the rotational velocity $v(r)$ with the distance r to the galactic center that would be expected in the absence of dark matter. The conclusion based on these observations was that dark matter dominates the dynamics not just of galaxy clusters but also of individual galaxies as well [6, 7].

Throughout the 1940s, more extensive observations were made of the M31 rotation curve as well as that of the spiral galaxy M33 [8, 9]. Also, a significant change in the distance estimate for M31 occurred, as reviewed in ref. [10]. However, these developments *left intact* the conclusion that dark matter dominates the structure and dynamics of both individual galaxies as well as galaxy clusters [10].

In the 1950s, radio observations of atomic hydrogen gas clouds at 21 cm wavelength in Milky Way and M31 confirmed the flat rotation curve of M31 and provided evidence for a flat rotation curve in the Milky Way [11, 12]. In August 1961, the International Astronomical Union hosted a special meeting focused on the observational evidence that dark matter dominates the structure and dynamics of galaxy clusters within an expanding universe cosmology [13]. In the early 1960s, analysis of the motion of some of the brightest and hottest stars in the Milky Way — so-called early-type stars which fall in spectral classes O and B — provided further evidence for our galaxy’s flat rotation curve [14, 15].

The discovery of the cosmic microwave background in 1965 provided strong independent observational support for an expanding universe [16, 17]. But the dark matter solution to the scatter observed in galaxy clusters around the cosmological redshift-distance relation for galaxies in an expanding universe creates a corresponding dark matter problem in astroparticle physics: *What is the particle nature of the dark matter?* Analysis of light element nucleosynthesis in the context of an expanding universe cosmology [18] when combined with observational estimates of the “primordial” deuterium abundance [19] strongly suggested by the late 1970s that dark matter does *not* contain significant quantities of protons or other atomic nuclei [20–23].

This Article presents a solution to the dark matter problem in astroparticle physics within the context of an expanding universe cosmology. The solution begins with the proposal of a model for quantum chromodynamic (QCD) axion dark matter with rest-mass energy around 0.5 eV in Sec. 2. The model assumes that 0.5 eV QCD axion dark matter comes in as many kinds or flavors as the number of flavors of matter in the standard model of particle physics. For each of the *twelve* flavors of quark and of leptons in the standard model [24], we make a model for 0.5 eV QCD axion dark matter with the corresponding flavor.

Based on this model, a cosmological argument is given for the rest-mass energy of 0.5 eV QCD axion dark matter in Sec. 3. The argument assumes that dark matter is made entirely of QCD axions with rest-mass energy around half of an electron-Volt. With this assumption, the argument then leads to a percent-level precision prediction for the actual 0.5 eV QCD axion dark matter rest-mass energy. The percent-level precision of the cosmological prediction for the 0.5 eV QCD axion dark matter rest-mass energy is set by the percent-level precision of the best available estimate of the present energy density of dark matter within the standard

expanding universe cosmology [25].

In Sec. 4, a direct determination of the 0.5 eV QCD axion dark matter rest-mass energy to 44 parts per million is presented. The determination is based on the analysis of fixed target photoproduction experiments. The experimentally determined value for the 0.5 eV QCD axion dark matter rest-mass energy is found to agree within a percent with the cosmological prediction.

The agreement between the cosmological prediction and the experimental determination of the rest-mass energy of the 0.5 eV QCD axion dark matter is taken as evidence demonstrating that dark matter is indeed made of 0.5 eV QCD axions described by the proposed model. Cosmological and astroparticle implications of the 0.5 eV QCD axion dark matter are then discussed in Sec. 5. Finally, in Sec. 6, answers are given to three burning questions in cosmology and astroparticle physics posed by 0.5 eV QCD axion dark matter.

2 0.5 eV QCD Axion Dark Matter Model

The model of the 0.5 eV QCD axion dark matter A_M with flavor M can be expressed in similar terms as the familiar constituent quark models for hadrons. In particular, the lightest neutral hadron — denoted π^0 and referred to as the neutral pion — has the same space-time symmetry properties as the axion A_M [26–28]. It is invariant under spatial rotations and space-time boosts, odd under spatial-inversion $\mathcal{P}A_M = -A_M$, odd under time-reversal $\mathcal{T}A_M = -A_M$, and even under charge-conjugation $\mathcal{C}A_M = A_M$ [24].

Recall that the constituent quark model for the neutral pion takes the simple form [24]

$$\begin{aligned}\pi^0 &= (u\bar{u} - d\bar{d})/\sqrt{2}, \\ &= (u_L\bar{u}_R - u_R\bar{u}_L)/2 - (d_L\bar{d}_R - d_R\bar{d}_L)/2\end{aligned}\quad (2.1)$$

where u is the up quark, d is the down quark, and \bar{M} is the anti-quark of the quark with flavor M . The meaning of the notation is that the neutral pion can be regarded for isospin-symmetry purposes as a bound state of a quark and anti-quark. The bound state has an equal chance — but opposite amplitude — for the flavor of the quark to be up or down.

We seek a model for the 0.5 eV QCD axion dark matter A_M for each flavor M of quark and each flavor of lepton in the standard model of particle physics. Therefore, we cannot use a superposition of flavor eigenstates as in Eq. (2.1). Instead, we introduce a new quantum number P which we refer to as *chirality*. The chirality $P = +$ is positive for matter or antimatter that does not feel the weak nuclear force. Conversely, the chirality $P = -$ is negative for matter or antimatter that feels the weak nuclear force.

2.1 Chirality and Helicity: What's the Difference?

Conceptually, the chirality index $P = \pm$ is distinct from the helicity $H = L, R$. Here, we have in mind *massless* matter and antimatter fields. Then, right-handed helicity R means that the spin points along the linear momentum. Similarly, left-handed helicity L means the spin points opposite to the linear momentum.

One can easily imagine a right-handed matter field of flavor M that feels the weak nuclear force. In our notation, such a field is denoted M_R^+ . Its antiparticle in the same notation is \bar{M}_L^+ . This means the antiparticle has the same flavor M and chirality $P = -$ but opposite helicity $H = L$. The chirality $P = -$ indicates that both particle M_R^+ and the antiparticle

\overline{M}_L^- feel the weak nuclear force. The flip in helicity means the antiparticle is left-handed when the particle is right-handed.

However, in the standard model of particle physics, there is a correlation between helicity and chirality [29, 30]. In the standard model, only left-handed matter and right-handed antimatter feel the weak nuclear force. Right-handed matter and left-handed antimatter do not feel it. In our notation, left-handed standard model matter is M_L^- and has chirality $P = -$ to indicate that it feels the weak nuclear force. By contrast, right-handed standard model matter is M_R^+ and has chirality $P = +$ to indicate that it does not feel the weak nuclear force.

To make the model of 0.5 eV QCD axion dark matter, then, we have gone beyond the standard model of particle physics. We include “normal” left-handed matter M_L^- that feels the weak nuclear force and “normal” right-handed matter M_R^+ that does not feel it along with their antiparticles. Similarly included are right-handed “normal” antimatter \overline{M}_R^- which feels the weak nuclear force and left-handed “normal” antimatter \overline{M}_L^+ which does not feel it. But also, we allow “mirror” matter (M_L^+ and M_R^-) as well as “mirror” antimatter (\overline{M}_R^+ and \overline{M}_L^-).

We note that mirror matter has the same correlation between helicity $H = L, R$ and chirality $P = \pm$ as normal antimatter. Left-handed mirror matter M_L^+ and left-handed normal antimatter \overline{M}_L^+ both do not feel the weak nuclear force, while right-handed mirror matter M_R^- and right-handed normal antimatter \overline{M}_R^- both feel it. Similarly, normal matter has the same correlation between helicity and chirality as mirror antimatter. Left-handed normal matter M_L^- and left-handed mirror antimatter \overline{M}_L^- both feel the weak nuclear force, while right-handed normal matter M_R^+ and right-handed mirror antimatter \overline{M}_R^+ both do not feel it.

In a sense, we have doubled the matter content of the standard model while keeping fixed the gauge fields which couple to the matter fields. Photons still carry electromagnetism described by quantum electrodynamics [31–37]. Gluons still carry the strong nuclear force described by QCD [38, 39]. The charged W^\pm and neutral Z^0 weak vector bosons still carry the weak nuclear force [40–42]. The only change is that we now admit both of the logical possibilities for the correlation between chirality $P = \pm$ and helicity $H = L, R$. To build 0.5 eV QCD axion dark matter we need both normal matter and mirror matter as well as their antiparticles.

2.2 Continuous $U(1)_A$ Axial Phase Symmetry

In effect, we have introduced a new continuous $U(1)_A$ axial phase symmetry $U_A(\alpha)$ with real parameter α . The axial phase lets us distinguish normal matter from mirror matter using symmetry:

$$\begin{aligned} U_A(\alpha)M_L^- &= \exp(-i\alpha)M_L^- \\ U_A(\alpha)M_R^+ &= \exp(+i\alpha)M_R^+ \\ U_A(\alpha)M_L^+ &= \exp(+i\alpha)M_L^+ \\ U_A(\alpha)M_R^- &= \exp(-i\alpha)M_R^-, \end{aligned} \tag{2.2}$$

where the first two lines are for normal matter and the last two lines are for mirror matter. The corresponding conserved charge is the axial charge $Q_A = P$ given by the chirality P for matter. Antimatter with chirality P has the opposite axial charge $Q_A = -P$. In terms of the

chirality P , the continuous $U(1)_A$ axial phase symmetry takes the simple form

$$\begin{aligned} U_A(\alpha)M_H^P &= \exp(iP\alpha)M_H^P \\ U_A(\alpha)\overline{M}_H^P &= \exp(-iP\alpha)\overline{M}_H^P. \end{aligned} \quad (2.3)$$

2.3 Discrete Space-Time Symmetries: \mathcal{P} , \mathcal{C} , \mathcal{T} and All That

To construct 0.5 eV QCD axion dark matter A_M , the transformation properties of the normal matter and mirror matter fields M_H^P , as well as their antiparticles \overline{M}_H^P , under the discrete space-time symmetries of space-inversion \mathcal{P} , charge-conjugation \mathcal{C} , and time-reversal \mathcal{T} are essential. We will find that the form of the axion A_M is essentially determined by these properties. In our notation, the discrete space-time symmetries act as follows:

$$\begin{aligned} \mathcal{P}M_H^P &= M_{\overline{H}}^{\overline{P}} & \mathcal{P}\overline{M}_H^P &= \overline{M}_{\overline{H}}^{\overline{P}} \\ \mathcal{C}M_H^P &= \overline{M}_H^{\overline{P}} & \mathcal{C}\overline{M}_H^P &= M_H^{\overline{P}} \\ \mathcal{T}M_H^P &= \overline{M}_H^P & \mathcal{T}\overline{M}_H^P &= M_H^P, \end{aligned} \quad (2.4)$$

where the notation $\overline{P} = -P$ indicates a flip of chirality and similarly \overline{H} means we flip helicity so that $\overline{L} = R$ and $\overline{R} = L$.

Three key features of the discrete space-time symmetries determine the form of the transformation given in Eq. (2.4). First, space-inversion flips helicity H since linear momentum is even under space-inversion but spin is odd under \mathcal{P} . However, the weak nuclear force breaks space-inversion \mathcal{P} [29, 30]. Given the correlation between helicity H and chirality P for both normal and mirror fields, this means that chirality P must also flip under space-inversion to insure that matter which feels the weak nuclear force is interchanged with matter that does not feel this force. Since space-inversion takes matter into matter and antimatter into anti-matter, these features suffice to determine the form of \mathcal{P} given in Eq. (2.4).

Second, charge-conjugation interchanges matter with antimatter and it is also broken by the weak interaction [29, 30]. In our notation, it follows that the chirality P must flip under \mathcal{C} to take fields that feel the weak nuclear force into fields that do not feel it. However, helicity H is unchanged. Combining these features, we obtain the \mathcal{C} transformation law shown in Eq. (2.4).

Third, the product \mathcal{PCT} of all three symmetries is the identity in the sense that $\mathcal{PCT}M_H^P = M_H^P$ and $\mathcal{PCT}\overline{M}_H^P = \overline{M}_H^P$. This relation is respected by all three gauge couplings in the standard model and has been observed to hold experimentally to high precision for a wide variety of particle properties including charge, mass, life-time, magnetic dipole moment, and so on, for a wide range of particles [43]. The transformation law for \mathcal{T} in Eq. (2.4) is then fixed by simply requiring $\mathcal{T} = \mathcal{PC}$ and using the laws for \mathcal{P} and \mathcal{C} given in Eq. (2.4). We find \mathcal{T} reverses helicity H , exchanges matter for antimatter, and leaves unchanged chirality P .

2.4 0.5 eV QCD Axion Dark Matter at Last

Having gone beyond the standard model of particle physics by introducing mirror matter and mirror antimatter, we now build the 0.5 eV QCD axion dark matter model. As advertised, the model takes the form of the constituent quark models for hadrons such as that of the neutral pion π^0 given in Eq. (2.1). Up to a normalization factor, the axion with flavor M is simply

$$A_M = M_L^-\overline{M}_R^+ - M_R^+\overline{M}_L^- + M_R^-\overline{M}_L^+ - M_L^+\overline{M}_R^-, \quad (2.5)$$

where the meaning of the notation is that the axion has the same continuous axial phase symmetry properties as a bound state of normal matter and mirror antimatter — given by the first two terms — that is “resonating” with a bound state of normal antimatter and mirror matter given by the last two terms. We emphasize that there is one axion A_M for each of the *twelve* flavors M of quark and of lepton in the standard model of particle physics [24].

The form of the 0.5 eV QCD axion dark matter A_M in Eq. (2.5) is essentially fixed by the space-time symmetries of the axion [26–28]. Each term combines matter and antimatter with the same flavor M but with opposite helicity H and chirality P . The helicity structure is identical with the neutral pion π^0 within the quark model in Eq. (2.1). From the fact that π^0 has zero spin and obeys Bose-Einstein statistics, it then follows that 0.5 eV QCD axion dark matter A_M in Eq. (2.5) has zero spin and obeys Bose-Einstein statistics [26–28].

Meanwhile, the signs and the equal size of the terms in the 0.5 eV QCD axion dark matter A_M in Eq. (2.5) are determined by the requirement that it transform in the same way as π^0 under space-inversion $\mathcal{P}A_M = -A_M$ and charge-conjugation $\mathcal{C}A_M = +A_M$ [26–28]. Using the representation of space-inversion symmetry \mathcal{P} given in the first line of Eq. (2.4), we find that space-inversion \mathcal{P} swaps the first two terms with one another and the last two terms with each other. Similarly, using the representation of charge-conjugation symmetry given in the second line of Eq. (2.4), we find that charge-conjugation \mathcal{C} swaps the first and third terms with one another and the second and fourth terms with each other. Therefore, all the terms in the expression for 0.5 eV QCD axion dark matter axion A_M must enter with equal size and with the pattern of signs shown in Eq. (2.5).

2.5 An Instanton Comment on 0.5 eV QCD Axion Dark Matter

We comment that the “resonance” of the axion A_M in Eq. (2.5) between the first two terms and the last two terms breaks the continuous axial phase symmetry $U_A(\alpha)$ given in Eq. (2.2). In fact, the resonance changes the axial charge $\Delta Q_A = \pm 4$ by four. This resonance is an instanton effect [44, 45] due to finite-action gauge field configurations in imaginary time with Pontryagin class $q = \pm 1$ [46].

Physically, the origin of the resonance inside the axion A_M in Eq. (2.5) comes from the fact that the instanton binds to itself certain “fermion zero modes” [44, 45]. These are zero energy solutions of the Dirac equation for matter fields in the presence of the instanton gauge-field configuration. The fermions are localized near the point in space-time where the instanton sits.

In the presence of the flow of axial charge from the fields inside an axion, the fermion zero modes mix [44, 45]. The mixing lets the fields inside the axion change their axial charge $\Delta Q_A = \pm 4$ by creating a compensating change in the axial charge of the fermion zero modes bound to the instanton. In effect, matter fields pass “through the mirror” in the presence of the instanton. In doing so, normal matter and mirror matter interchange with one another. So also, normal antimatter and mirror antimatter interchange with each other.

In principle, one could estimate the rest-mass energy $m_A c^2 \approx 0.5$ eV of the 0.5 eV QCD axion dark matter from this instanton effect [45]. However, the growth of the strong coupling constant $\alpha_s(Q)$ with decreasing momentum transfer Q prevents a controlled perturbative calculation in the relevant regime of small momentum transfer $Q = m_A c^2 \ll \Lambda_{\text{QCD}}$ compared to the scale $\Lambda_{\text{QCD}} \approx 100$ MeV where $\alpha_s(\Lambda_{\text{QCD}})$ becomes large [38, 39]. Still, a formal analysis of the fermion zero mode mixing due to the axial charge flow within the axion is possible [47, 48].

In short, the 0.5 eV QCD axion dark matter model presented in Eq. (2.5) leads to mixing between fermion zero modes that solves the so-called Strong CP problem [47–49]. Instead of a controlled perturbative calculation leading to a direct result for the 0.5 eV QCD axion dark matter rest-mass, one must resort to current algebra techniques or to an effective lagrangian approach [26, 27, 49, 50]. The result is the following link between the axion rest-mass energy $m_A c^2$ and the axion decay constant f_A using the topological susceptibility χ_{QCD} of the QCD vacuum [26, 27, 49, 50]:

$$m_A c^2 f_A = \sqrt{\chi_{\text{QCD}}} = (5.69 \pm 0.05) \times 10^{-3} \text{ GeV}^2. \quad (2.6)$$

Both methods are based on the symmetry of the QCD lagrangian under the continuous $U(1)_A$ axial phase symmetry in Eq. (2.2) combined with the breaking of this symmetry by the 0.5 eV QCD axion dark matter A_M in Eq. (2.5). In Eq. (2.6), we have used the best present available result for χ_{QCD} which comes from the effective lagrangian approach [50].

2.6 Summary: There are Twelve Flavors of 0.5 eV QCD Axion Dark Matter

To get a percent-level precision prediction for the rest-mass energy $m_A c^2 \approx 0.5$ eV of the 0.5 eV QCD axion dark matter described by the model in Eq. (2.5), we now take a cosmological turn. The next section presents a simple cosmological argument that leads to the percent-level precision prediction $m_A c^2(\text{Theory}) = (0.508 \pm 0.004)$ eV based on the best present estimate for the cosmological energy density of dark matter within the standard expanding universe cosmology [25]. The cosmological argument is rooted in the straightforward fact that there are *twelve* 0.5 eV QCD axion dark matter flavors A_M described by Eq. (2.5). This fact follows from the experimental fact that there are *twelve* flavors M of quarks and of leptons in the standard model of particle physics [24] and from the explicit construction in this section of 0.5 eV QCD axion dark matter A_M for each such flavor M (See Eq. (2.5)).

3 0.5 eV QCD Axion Dark Matter Rest-Mass Energy Prediction

In this section we present a cosmological argument leading to the percent-level precision prediction for the rest-mass energy of 0.5 eV QCD axion dark matter:

$$m_A c^2(\text{Theory}) = (0.508 \pm 0.004) \text{ eV}, \quad (3.1)$$

where the percent-level uncertainty derives from the best present estimate of the cosmological energy density parameter of dark matter $\Omega_{\text{DM}} h^2 = 0.11882 \pm 0.00086$ [25] within the standard expanding universe cosmology. As a first step, we indulge in a little circular logic and simply compute the axion decay constant using the result for the axion rest-mass energy in Eq. (3.1) which we seek to derive from cosmology:

$$f_A(\text{Theory}) = \frac{\sqrt{\chi_{\text{QCD}}}}{m_A c^2(\text{Theory})} = (1.120 \pm 0.013) \times 10^7 \text{ GeV}, \quad (3.2)$$

where we have used the relation in Eq. (2.6) to find the axion decay constant given the prediction for the 0.5 eV QCD axion dark matter rest-mass energy. The point of this computation is that the 0.5 eV QCD axion dark matter decay constant is roughly 11,200 Tera electron-Volts, give or take one percent. This fundamental energy scale is *more than 100 times higher* than the highest center-of-mass-frame collision energy $\sqrt{s} \approx 100$ TeV of any particle collider that has yet reached the conceptual design phase [51].

In what follows, we will assume that 0.5 eV QCD axion dark matter has rest-mass energy roughly 0.5 eV and that the axion decay constant is given roughly by the value in Eq. (3.2). We will argue in subsection 3.1 that the *massless* mirror matter and *massless* mirror antimatter within the 0.5 eV QCD axion dark matter remain confined all the way back to the moment of the Big Bang itself. Then, in subsection 3.2, we will estimate the temperature of the Big Bang itself and compare the resulting energy scale with the much larger value of the axion decay constant in Eq. (3.2). From the comparison, we will reaffirm the conclusion that the *massless* mirror matter and *massless* normal matter found inside 0.5 eV QCD axion dark matter remain confined throughout the evolution of the expanding universe from the moment of the Big Bang to the present. Finally, in subsection 3.3, we derive the rest-mass energy of 0.5 eV QCD axion dark matter by assuming that it forms all of the dark matter in the present universe.

3.1 Massless Mirror Matter Confined within 0.5 eV QCD Axion Dark Matter

Given the large energy scale for the axion decay constant, it is safe to assume that the *massless* mirror matter and *massless* mirror antimatter found within the 0.5 eV QCD axion dark matter are in fact confined within the axion. The safety comes from the relatively low energy scales considered in our cosmological argument. The primary energy scale that we consider in the present universe, for example, is the present energy per photon in the cosmic microwave background (CMB) (See ref. [52], pg. 134–138,158):

$$\begin{aligned} u_\gamma/n_\gamma &= \left(\frac{3! \zeta(4)}{\pi^2} \frac{(kT_\gamma)^4}{(\hbar c)^3} \right) / \left(\frac{2! \zeta(3)}{\pi^2} \frac{(kT_\gamma)^3}{(\hbar c)^3} \right) \\ &= 2.701 kT_\gamma \\ &= (6.3437 \pm 0.0016) \times 10^{-4} \text{ eV}, \end{aligned} \quad (3.3)$$

where u_γ is the present photon energy density, n_γ is the present photon number density, and $T_\gamma = (2.7255 \pm 0.0006)$ K [53] is the present photon temperature.

The present energy per photon in the CMB given in Eq. (3.3) sets the characteristic kinetic energy per particle for particle dark matter in the universe today. It is far smaller than the energy scale set by the axion decay constant in Eq. (3.2). Therefore, it is safe to assume that the *massless* mirror matter and *massless* mirror antimatter found within the 0.5 eV QCD axion dark matter according to our model in Eq. (2.5) remain confined within the axion in the present universe. In fact, we will assume that the 0.5 eV QCD axion dark matter is *cold* in the sense that we can even neglect its kinetic energy — given roughly by the energy per photon in the CMB in Eq. (3.3) — in comparison with the QCD axion dark matter’s 0.5 eV rest-mass energy.

The next higher energy scale we will consider in the cosmological argument for the 0.5 eV rest-mass energy of QCD axion dark matter is set by the redshift $z_{\text{eq}} = 3376 \pm 19$ [25] of so-called matter-radiation equality. At redshift z_{eq} , the average photon energy in the cosmic background radiation (CBR) is roughly z_{eq} times larger than present average photon energy in the CMB (ref. [52], pg. 71, 96). The result is comparable to the 0.5 eV rest-mass energy of QCD axion dark matter, but it is still much smaller than the axion decay constant given in Eq. (3.2). Again, the *massless* mirror matter and mirror antimatter are safely confined within 0.5 eV QCD axion dark matter even at the epoch of “matter-radiation equality” in the standard expanding universe cosmology [25].

Finally, at the upper end, the highest energy scale we consider in the cosmological argument is the moment of the Big Bang itself. We assert that this is precisely the moment

of confinement of *massless* mirror matter and *massless* mirror antimatter within 0.5 eV QCD axion dark matter. Prior to the Big Bang, there is no 0.5 eV QCD axion dark matter. After the Big Bang, there is 0.5 eV QCD axion dark matter.

At the Big Bang itself, 0.5 eV QCD axion dark matter forms through the binding of *massless* mirror matter to *massless* normal antimatter. This pattern of binding resonates with its “mirror” reflection in which *massless* mirror antimatter binds to *massless* normal matter. In this way, the *massless* matter and antimatter — both normal and mirror — is confined inside 0.5 eV QCD axion dark matter at the moment of the Big Bang.

3.2 Big Bang Temperature from QCD Axion Angle Jump $\Delta\theta_A = \pi$

To corroborate our assertion that *massless* quarks and leptons remain confined inside 0.5 eV QCD axion dark matter right up to the Big Bang itself, we now estimate the energy scale of the Big Bang using an analysis motivated by the continuous $U(1)_A$ axial phase symmetry given in Eq. (2.2). Before the Big Bang, there is no 0.5 eV QCD dark matter to break this symmetry. Instead, the deconfined *massless* quarks and leptons — both normal and mirror — conserve axial charge Q_A in all their interactions. The continuous $U(1)_A$ axial phase symmetry thus emerges along with the closing of the mass gap in the spectrum of particles.

Topologically, this critical phase before the Big Bang lives on the space-like three-dimensional boundary of our four-dimensional expanding universe space-time. On the boundary of space-time, then, we find an emergent continuous $U(1)_A$ axial phase symmetry. By contrast, in the four-dimensional bulk of space-time, the continuous $U(1)_A$ axial phase symmetry is broken by 0.5 eV QCD axion dark matter. Moreover, on the boundary, *massless* quarks and leptons move freely and are deconfined. In the bulk, by contrast, the *massless* quarks and leptons are confined inside the 0.5 eV QCD axion dark matter.

Physically, the gaplessness of the quarks and leptons on the boundary of space-time and the emergence of the continuous $U(1)_A$ axial phase symmetry there are protected by a jump $\Delta\theta_A = \pi$ in the value of the axion “angle” θ_A [49]. Using the topological susceptibility of the QCD vacuum quoted in Eq. (2.6), we can estimate the kinetic energy density of 0.5 eV QCD dark matter at the Big Bang from the jump $\Delta\theta_A = \pi$ in the axion angle:

$$u_A(T_\pi) = \chi_{\text{QCD}} \left(\frac{\Delta\theta_A}{6} \right)^2 = 7 \frac{3! \zeta(4)}{\pi^2} ((37.26 \pm 0.16) \text{ MeV})^4, \quad (3.4)$$

where we have assumed that the energy-scale $kT_\pi = (37.26 \pm 0.16)$ MeV set by the temperature of the Big Bang is much larger than the 0.5 eV rest-mass energy of 0.5 eV QCD axion dark matter.

In detail, we used the fact that the 0.5 eV QCD axion dark matter in Eq. (2.5) has *twelve* flavors, spin zero, and Bose-Einstein statistics to relate its kinetic energy density to the temperature of the Big Bang (See ref. [52], pg. 134–138, 158). This gives the factor of seven on the right-hand side of Eq. (3.4) which has been normalized to the photon energy density. Here, the seven reflects the fact that there are *six* axions for every photon and that the kinetic energy of the photons and axions together soaks up the potential energy released when the axion angle jumps $\Delta\theta_A = \pi$ at the Big Bang.

The factor of six in the denominator on the left-hand side of Eq. (3.4) is simply the number of flavors of quarks. This factor follows from the conventional normalization of the axion-gluon coupling together with the form of the continuous $U(1)_A$ axial phase symmetry given in Eq. (2.3) [28, 49]. The symmetry acts in the same way on all flavors M of quarks and this leads to the factor of six in the denominator on the right-hand side of Eq. (3.4).

We conclude the energy-scale $kT_\pi = (37.26 \pm 0.16)$ MeV set by the temperature of the Big Bang is still much smaller than the energy-scale set by the axion decay constant given in Eq. (3.2). It follows that there is indeed no point in the evolution of the expanding universe since the Big Bang when 0.5 eV QCD dark matter had the kinetic energy needed to break *massless* mirror matter and *massless* mirror antimatter free from their confinement. We feel that it is therefore safe to focus on the cosmological effects of the 0.5 eV QCD axion dark matter itself. Remarkably, this cosmological focus allows one to predict the rest-mass energy of the 0.5 eV QCD axion dark matter with percent-level precision provided that it forms all of the dark matter in the present universe.

3.3 0.5 eV QCD Axion Dark Matter Rest-Mass Energy Prediction at Last

At last we present the cosmological argument for the rest-mass energy given in Eq. (3.1) for the 0.5 eV QCD axion dark matter in Eq. (2.5). We have already extensively used our assumption that the rest-mass energy of the 0.5 eV QCD axion dark matter is around 0.5 eV in the previous two subsections. However, the fact that all of the dark matter in the present universe is made of 0.5 eV QCD axion dark matter has not yet been put in play. Let us do so now.

Assuming that 0.5 eV QCD dark matter is all of the dark matter in the present universe, it is straightforward to compute the rest-mass energy given in Eq. (3.1):

$$\begin{aligned}
m_A c^2(\text{Theory}) &= \frac{u_A(T_\gamma)}{n_A(T_\gamma)} \\
&= \frac{n_\gamma}{n_A(T_\gamma)} \frac{u_\gamma}{n_\gamma} \frac{\Omega_{\text{DM}} h^2}{\Omega_\gamma h^2} \\
&= \frac{1}{6} (2.701 kT_\gamma) \frac{\Omega_{\text{DM}} h^2}{\Omega_\gamma h^2} \\
&= (0.508 \pm 0.004) \text{ eV,}
\end{aligned} \tag{3.5}$$

where we have used Eq. (3.3) for the average energy per photon $u_\gamma/n_\gamma = 2.701 kT_\gamma$ in the present universe and we have treated the 0.5 eV QCD axion dark matter as *cold* by dropping the kinetic energy contribution to the present energy density $u_A(T_\gamma) \approx n_A(T_\gamma)m_A c^2$. Here, the photon cosmological energy density parameter is $\Omega_\gamma h^2 = (8\pi/3)(G/c^2)(h/H_0)^2 u_\gamma = 2.473 \times 10^{-5}$ (See [52] pg. 100, 102–103). Similarly, the best present estimate of the dark matter energy density parameter is $\Omega_{\text{DM}} h^2 = (8\pi/3)(G/c^2)(h/H_0)^2 u_A(T_\gamma) = 0.11882 \pm 0.00086$ [25].

We have assumed that dark matter is made of 0.5 eV QCD axion dark matter. But, the key step in the argument clearly comes in the passage from the second to the third line in Eq. (3.5). It asserts that there are *six* 0.5 eV QCD axions for each photon in the CMB so that $n_A(T_\gamma)/n_\gamma = 6$.

We now argue there are, in fact, *six* 0.5 eV QCD axions for each photon in the CMB. Indulging again in a bit circular reasoning, we assume that the rest-mass energy of the 0.5 eV QCD axion dark matter is around 0.5 eV. But now we are also assuming that it forms all of the dark matter. With those two assumptions, we can simply compute the present number density of 0.5 eV QCD axions by reversing the key step in Eq. (3.5)

$$n_A(T_\gamma) \approx 6n_\gamma. \tag{3.6}$$

Let us then walk back in time from the present universe to the Big Bang. Since the axion decay constant given in Eq. (3.2) is much larger than the energy scale set by even

the temperature of the Big Bang itself in Eq. (3.4), it follows that the axion-to-photon ratio has remained fixed throughout the evolution of the universe since the Big Bang to good approximation. But at the Big Bang itself, the ratio is simply determined by the ratio $g_A/g_\gamma = 12/2 = 6$ of the statistical degeneracy factor $g_A = 12$ for the axion and that for the photon $g_\gamma = 2$ (See ref. [52], 137, 158–159). We emphasize that the statistical degeneracy $g_A = 12$ of the 0.5 eV QCD axion dark matter follows from the fact that there are *twelve* flavors of these spin zero particles and that they obey Bose-Einstein statistics.

In conclusion, we can simply replace the \approx symbol in Eq. (3.6) with an $=$ sign. The cosmological derivation of the rest-mass energy of the 0.5 eV QCD axion dark matter is now complete. The key step was to use the fact that there are *twelve* flavors of 0.5 eV QCD axion dark matter to deduce that there are *six* such axions for every photon in the CMB.

3.4 Comment on Axion-Photon Coupling of 0.5 eV QCD Axion Dark Matter

Having derived a prediction for the rest-mass energy of 0.5 eV QCD axion dark matter with percent-level precision in Eq. (3.5), we pause to comment on the corresponding prediction for the strength of the axion-photon coupling that follows from this result [28, 49]. We recall that the axion field ϕ_A couples linearly to the dot product $\mathbf{E} \cdot \mathbf{B}$ of the electric field \mathbf{E} and the magnetic field \mathbf{B} . In units where $\hbar = c = 1$, this linear coupling has strength $g_{A\gamma\gamma}$ and the Lagrangian density takes the simple form [28, 49]

$$\mathcal{L}_{A\gamma} = g_{A\gamma\gamma} \phi_A \mathbf{E} \cdot \mathbf{B}, \quad (3.7)$$

where $g_{A\gamma\gamma} f_A = (\alpha/2\pi) C_{A\gamma}$ determines the axion-photon coupling in terms of the axion decay constant f_A , the electromagnetic “fine-structure” coupling constant is $\alpha = e^2/(\hbar c 4\pi\epsilon_0) \approx 1/137$, and the dimensionless constant $C_{A\gamma} = 8/3 - (8m_d + 2m_u)/(3m_d + 3m_u) = 0.653 \pm 0.017$ [28, 49] is fixed by the best present determination of the light-quark mass ratio $m_u/m_d = 0.485 \pm 0.019$ [54] and by the fact that all flavor M of quarks and of leptons transform in the same way under the continuous $U(1)_A$ axial phase symmetry in Eq. (2.2).

Using the value for the axion decay constant in Eq. (3.2), we find the percent-level precise prediction for the strength of the axion-photon coupling for 0.5 eV QCD axion dark matter

$$g_{A\gamma\gamma}(\text{Theory}) = (0.68 \pm 0.02) \times 10^{-10} \text{ GeV}^{-1}. \quad (3.8)$$

We can use this to estimate the lifetime of 0.5 eV QCD axion dark matter due to the spontaneous decay of the axion into a pair of photons:

$$\begin{aligned} \tau_A &= \tau_\pi \left(\frac{1}{C_{A\gamma}} \right)^2 \left(\frac{f_A}{f_\pi} \right)^2 \left(\frac{m_\pi}{m_A} \right)^3 \\ &= (1.81 \pm 0.10) \times 10^8 \frac{h}{H_0}, \end{aligned} \quad (3.9)$$

where $\tau_\pi = (8.43 \pm 0.13) \times 10^{-17} \text{ sec} / (0.98823) = (8.53 \pm 0.13) \times 10^{-17} \text{ nsec}$ [24] is the two-photon lifetime of the neutral pion π^0 , $f_\pi = (1/\sqrt{2})(127.13/0.974) = 92.3 \text{ MeV}$ [24] is the pion decay constant, and $m_\pi = 134.98 \text{ MeV}$ [24] is the rest-mass energy of the neutral pion π^0 .

Here, we have compared the axion lifetime to the typical time-scale from cosmology $h/H_0 = 3.09 \times 10^{17} \text{ sec}$ (ref. [52], pg. 25, 102–103). This time-scale is roughly comparable to the best available estimate of the present age of the universe within the standard expanding

universe cosmology [25]. The conclusion is that spontaneous axion decay to a pair of photons is strongly suppressed by the large axion decay constant of 0.5 eV QCD axion dark matter. This supports our cosmological argument which asserts that the axion-to-photon number ratio remains fixed from the Big Bang to the present.

3.5 Summary of 0.5 eV QCD Axion Rest-Mass Energy Prediction

In this section we have presented a cosmological argument for the rest-mass energy $m_A c^2 \approx 0.5$ eV of 0.5 eV QCD axion dark matter. The argument rested on two assumption. First, we assumed that the rest-mass energy is roughly 0.5 eV. Second, we assumed that 0.5 eV QCD axion dark matter forms all of the dark matter found in the present universe. On the basis of these two assumptions, the following percent-level precision prediction for the rest-mass energy of 0.5 eV QCD axion dark matter was derived:

$$m_A c^2(\text{Theory}) = (0.508 \pm 0.004) \text{ eV}.$$

In the next section, we justify these two assumptions by determining the rest-mass energy of 0.5 eV QCD axion dark matter to 44 parts per million precision and by finding that the value *agrees* with the percent-level prediction to better than a percent.

4 0.5 eV QCD Axion Dark Matter Rest-Mass Energy Determination

In the previous section, we assumed that 0.5 eV QCD axion dark matter forms all the dark matter in the universe and that it has rest-mass energy around $m_A c^2 \approx 0.5$ eV. With those two assumptions, we derived the percent-level precision prediction for the rest-mass energy $m_A c^2(\text{Theory}) = (0.508 \pm 0.004)$ eV. In the present section, we justify these two assumptions experimentally.

The argument justifying these assumptions consists in the experimental determination of the rest-mass energy of 0.5 eV QCD axion dark matter to 44 parts per million precision:

$$m_A c^2(\text{Experiment}) = (0.50580 \pm 0.00002) \text{ eV}. \quad (4.1)$$

We note that this agrees with the predicted value $m_A c^2(\text{Theory}) = (0.508 \pm 0.004)$ eV to within the percent-level precision of the comparison. On the basis of this agreement, we argue that 0.5 eV QCD axion dark matter forms all of the dark matter in the universe and that it has rest-mass energy around 0.5 eV.

4.1 Principle of 0.5 eV QCD Axion Dark Matter Photoproduction

The principle of the fixed target axion photoproduction experiments that we use to determine the rest-mass energy of 0.5 eV QCD axion dark matter can be described by the following set of reactions together with the corresponding equations expressing energy conservation [55]:

$$\begin{aligned} \gamma + \theta &\rightarrow A, & \nu_{A\theta} + \nu_\theta &= \nu_A \\ \gamma &\rightarrow \theta + A, & \nu_{A\theta} &= \nu_\theta + \nu_A \\ \gamma &\rightarrow \theta + 2A, & \nu_{A\theta} &= \nu_\theta + 2\nu_A, \end{aligned} \quad (4.2)$$

where the notation means that a photon γ with energy $h\nu_{A\theta}$ is absorbed in the fixed target with the production of an axion A with rest-mass energy $m_A c^2 = h\nu_A$. Here, the massive vector boson θ with rest-mass energy $h\nu_\theta$ represents a quantum of sound — known as an

optical phonon — that couples to light within the target material [56]. Physically, the mechanism for these reactions is that the dot product $\mathbf{E}_{A\theta} \cdot \mathbf{B}_\theta$ of the photon electric field $\mathbf{E}_{A\theta}$ with the phonon magnetic field \mathbf{B}_θ couples linearly to the axion field ϕ_A using the interaction shown in Eq. (3.7) [28, 49].

The linear coupling to the axion field ϕ_A turns the dot product $\mathbf{E}_{A\theta} \cdot \mathbf{B}_\theta$ into an “axion source” that makes 0.5 eV QCD axion dark matter. Crucially, the axion source need not make only one axion, as is shown in the first two lines in Eq. (4.2), but also the axion source can make a pair of axions, as is shown in the last line of Eq. (4.2). In all three cases, the conservation of energy then relates the photon beam energy $h\nu_{A\theta}$, the optical phonon rest-mass energy $h\nu_\theta$, and the axion rest-mass energy $m_A c^2 = h\nu_A$, as is shown in Eq. (4.2).

In the first reaction shown in Eq. (4.2), the photon from the beam collides with an optical phonon that has been excited within the fixed target by thermal fluctuations. The intensity of the axion photoproduction for this reaction therefore depends sensitively on the temperature of the material T . The thermal energy kT must be above — or at least not very below — the optical phonon rest-mass energy $h\nu_\theta$. In the second and third reactions shown in Eq. (4.2), the photon beam excites the optical phonon at the same time that it creates the axion or pair of axions.

4.2 0.5 eV QCD Axion Dark Matter Photoproduction Experimental Details

In this subsection we give the experimental details for the determination of the rest-mass energy of 0.5 eV QCD axion dark matter using fixed target photoproduction. The material of choice as the fixed target is the common plastic material polystyrene [57, 58]. Starting around 1950, thin films of polystyrene about 38 microns thick (one-thousandth of an inch) with a matte finish became the standard reference material for energy calibration of fixed target photoproduction experiments at photon beam energy from 0.05 eV to 0.5 eV [58–61]. As a result, the spectrum of optical phonon rest-mass energies $h\nu_\theta$ in the standard polystyrene calibration film is easily the best studied, most reliable, and most extensive of any known material [62].

The method of choice is infrared transmission spectroscopy [55]. Conventionally, infrared spectroscopy is broken into three domains according to the photon beam energy: Far-infrared from 0.005 eV to 0.05 eV, mid-infrared from 0.05 eV to 0.5 eV, and near-infrared from 0.5 eV to 1.5 eV. In all three domains of photon beam energy, the experimental principle remains the same: A beam of infrared light passes through a fixed target and the ratio $T(\nu_{A\theta})$ of the transmitted intensity to the incident intensity is measured as a function of the light frequency $\nu_{A\theta}$.

Figure 1 shows a typical photoproduction resonance in the mid-infrared spectrum of the standard calibration polystyrene thin film [57]. The spectrum was obtained on 18 April 2024 with a Thermo Scientific Nicolet iS50 Fourier transform infrared transmission spectrometer with potassium bromide (KBr) beamsplitter operated by Mr. Birk Dilebas in the laboratory of Prof. Jahan M. Dawlaty within the Department of Chemistry of the University of Southern California. The transmittance $T(\nu_{A\theta})$ was sampled within windows of photon beam energy of width $\Delta\nu_{A\theta} = 0.125 \text{ cm}^{-1}$. Both the polystyrene sample and the deuterated tri-glycine sulfate (DTGS) infrared detector were held at room temperature $T = (293 \pm 5) \text{ K}$. The sample chamber was partially purged of air before measurement. However, several sharp lines from residual atmospheric gases are still clearly visible riding on the broad polystyrene resonance line-shape shown in Fig. 1.

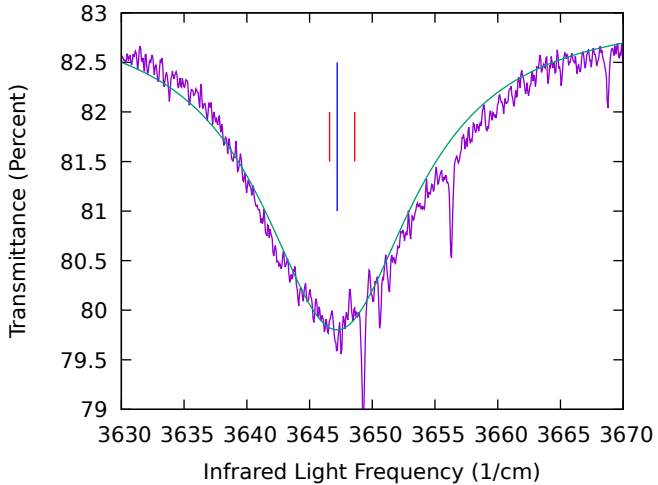


Figure 1. Polystyrene Axion Resonance—The infrared transmittance (rough purple curve) [55] through a thin film of the plastic material polystyrene [57] has a dip centered on the infrared light frequency $\nu_{A\theta}(1) \approx 3647.2 \text{ cm}^{-1}$ (long vertical blue line and smooth green line). Photons in the mid-infrared light with this frequency couple to the optical phonons in polystyrene with frequency $\nu_\theta(B) = (432 \pm 1) \text{ cm}^{-1}$ [64] to make dark matter in the form of axions with Compton frequency $\nu_A(I) = (4079.57 \pm 0.18) \text{ cm}^{-1}$ (See Table 3). The dip falls within the predicted window for the polystyrene axion resonance with frequency $\nu_{A\theta}(1) = \nu_A(I) - \nu_\theta(B) = (3647.6 \pm 1.0) \text{ cm}^{-1}$ (short vertical red lines).

To determine the photoproduction resonance frequency $\nu_{A\theta}(1) = 3647.2 \text{ cm}^{-1}$ for the polystyrene line shown in Fig. 1, a fit was made to the infrared transmittance $T(\nu_{A\theta})$ as a function of infrared photon frequency $\nu_{A\theta}$. A good fit was found using the standard narrow-resonance line-shape riding on top of a constant background:

$$T(\nu_{A\theta}) = A - B \frac{\Gamma^2}{(\nu_{A\theta} - \nu_{A\theta}(1))^2 + \Gamma^2}, \quad (4.3)$$

where $\Gamma = 7.4 \text{ cm}^{-1}$ is the half-width at half-maximum of the resonance line, $B = 3.2\%$ is the depth of the resonance, and $A = 83.0\%$ is the constant background. Systematic uncertainties due to photon beam energy calibration, beam energy resolution $\Delta\nu_{A\theta}$, sample and detector temperature T variation, and so on, were much smaller than the statistical uncertainty of the fit which was likely on the order of $\pm 1 \text{ cm}^{-1}$ for the resonance frequency $\nu_{A\theta}(1)$.

Table 1 lists the photon beam energies $h\nu_{A\theta}$ for six polystyrene fixed target photoproduction resonances in the mid-infrared and near-infrared [63]. Meanwhile, Table 2 does the same for five polystyrene optical phonon photoproduction resonances in the far-infrared and mid-infrared. Finally, in Table 3, we list four determinations of the 0.5 eV QCD axion dark matter rest-mass energy based on Eq. (4.2).

4.3 0.5 eV QCD Axion Dark Matter Rest-Mass Energy to 44 ppm At Last

The best present determination from the analysis of the near-infrared spectrum of polystyrene determines the 0.5 eV QCD axion rest-mass energy to 44 parts per million $m_A c^2(I) = h\nu_A(I) = (0.50580 \pm 0.00002) \text{ eV}$:

$$\nu_A(I) = \nu_{A\theta}(6) - \nu_{A\theta}(4) = (4079.57 \pm 0.18) \text{ cm}^{-1}, \quad (4.4)$$

Line	$\nu_{A\theta}$ (cm $^{-1}$)	Ref.
1	3647.6 ± 1.0	$\nu_A(I) - \nu_\theta(B)$
2	4331.58 ± 0.06	[63]
3	4621.8 ± 1.0	[63]
4	4663.27 ± 0.06	[63]
5	5946.70 ± 0.06	[63]
6	8742.84 ± 0.17	[63]

Table 1. Polystyrene Axion Lines—The infrared transmittance through the plastic material polystyrene dips at the axion resonance lines with frequencies $\nu_{A\theta}$ for room temperature and ambient pressure.

Phonon	ν_θ (cm $^{-1}$)	Ref.
A	247 ± 1	[64]
B	432 ± 1	[64]
C	542.2 ± 2.8	[62]
D	583.7 ± 0.2	$2\nu_{A\theta}(4) - \nu_{A\theta}(6)$
E	1871.6 ± 3.2	[60]

Table 2. Axion-Active Polystyrene Phonons—Optical phonons with frequencies ν_θ in the plastic material polystyrene at room temperature and ambient pressure couple to near-infrared light to make dark matter in the form of axions.

Axion	ν_A (cm $^{-1}$)	Comment
I	4079.57 ± 0.18	$\nu_{A\theta}(6) - \nu_{A\theta}(4)$
II	4084.6 ± 1.0	$\nu_{A\theta}(2) - \nu_\theta(A)$
III	4079.6 ± 3.0	$\nu_{A\theta}(3) - \nu_\theta(C)$
IV	4075.1 ± 3.2	$\nu_{A\theta}(5) - \nu_\theta(E)$

Table 3. Axion Compton Frequency Determinations—The Compton frequency of the axion $\nu_A = m_A c/h$ is determined by four independent analyses. The independent but consistent determinations are based on the polystyrene axion resonance frequencies $\nu_{A\theta}$ from Table 1 and the axion-active polystyrene phonon frequencies ν_θ from Table 2. Determination I gives the rest-mass of the axion $m_A(I) = h\nu_A(I)/c = (0.50580 \pm 0.00002)$ eV/c 2 to 44 parts per million precision.

where the resonance with frequency $\nu_{A\theta}(6) = 2\nu_A(I) + \nu_\theta(D) = (8742.84 \pm 0.17)$ cm $^{-1}$ [63] makes a pair of axions while the resonance with frequency $\nu_{A\theta}(4) = \nu_A(I) + \nu_\theta(D) = (4663.27 \pm 0.06)$ cm $^{-1}$ [63] makes just one axion. However, both resonances excite the same optical phonon which has the mid-infrared frequency

$$\nu_\theta(D) = 2\nu_{A\theta}(4) - \nu_{A\theta}(6) = (583.7 \pm 0.2) \text{ cm}^{-1}. \quad (4.5)$$

Indeed, a broad shoulder was seen in the polystyrene mid-infrared spectrum at roughly the predicted phonon frequency $\nu_\theta(D) \approx 580$ cm $^{-1}$ providing direct experimental confirmation of the interpretation of the near-infrared spectrum.

For further confirmation, we use our best present determination $\nu_A(I) = (4079.57 \pm 0.18)$ cm $^{-1}$ of the 0.5 eV QCD axion dark matter rest-mass from Eq. (4.4) to infer the

position of the line shown in Fig. 1:

$$\nu_{A\theta}(1) = \nu_A(I) - \nu_\theta(B) = (3647.6 \pm 1.0) \text{ cm}^{-1}, \quad (4.6)$$

where $\nu_\theta(B) = (432 \pm 1) \text{ cm}^{-1}$ [64] is the frequency of the relevant far-infrared optical phonon in polystyrene. This prediction is compared to the experimental determination in Fig. 1. We find that the predicted window in Eq. (4.6) includes the best fit value of the resonance frequency $\nu_{A\theta}(1) = 3647.2 \text{ cm}^{-1}$ for the line-shape in Eq. (4.3).

Finally, we note that the four independent determinations of the 0.5 eV QCD axion dark matter rest-mass energy shown in Table 3 agree with one another to within a tenth of a percent. This remarkable agreement involves the analysis and interpretation of five separate lines in the near-infrared polystyrene photoproduction spectrum shown in Table 1. Using our best determination of the rest-mass energy of 0.5 eV QCD axion dark matter to 44 parts per million precision in Eq. (4.4) and the second line of Eq. (4.2), we can predict to better than a tenth of a percent the resonance frequencies of the lines 2, 3, and 5 given the frequencies for their corresponding optical phonons A, C, and E in Table 2.

To the best of our knowledge, there does not exist a comparably precise and accurate prediction for the resonance frequencies of *any* near-infrared photoproduction line in *any* material — *including polystyrene*. More to the point, there does not seem to exist *any* pre-existing interpretation or assignment of the six polystyrene axion resonance lines shown in Table 1.

However, it should be emphasized that this is the general rule in *near*-infrared spectroscopy of liquid and solid materials. In this range of the infrared spectrum, the usual practice is instead to use the whole pattern of lines in the spectrum to identify the material [65]. In this context, our successful identification and interpretation of the polystyrene axion resonance lines is simply spectacular.

4.4 Confirmation of 0.5 eV QCD Axion Dark Matter Axion-Photon Coupling Strength

Experimental confirmation of the axion-photon coupling given in Eq. (3.8) is possible. The idea is to use the measured values of the axion resonance absorption coefficient

$$\alpha_{A\theta} = t^{-1} \log(T_{\text{bkg}}/T_{A\theta}). \quad (4.7)$$

Here, $t = 0.125 \text{ cm}$ is the thickness of the polystyrene samples, $T_{\text{bkg}} = 88\%$ is the frequency-independent background near-infrared transmittance, and $T_{A\theta}$ is the resonant transmittance in the *near*-infrared photoproduction experiments reported in ref. [63].

In detail, we focus on the axion resonance lines 4 and 6 in Table 1 which share the same axion-active phonon. As noted previously, resonance 6 creates two axions while resonance 4 creates just one. The predicted axion-photon coupling strength $g_{A\gamma\gamma} = (0.68 \pm 0.02) \times 10^{-10} \text{ GeV}^{-1}$ (See Eq. 3.8) then determines the ratio of the absorption coefficients:

$$\sqrt{\frac{\alpha_{A\theta}(6)}{\alpha_{A\theta}(4)}} = \sqrt{2} m_A c^2 g_{A\gamma\gamma} n S t = 0.286 \pm 0.008, \quad (4.8)$$

where the number density of polystyrene monomers is $n = \rho N_A / \mu = (1.04 \text{ g/cm}^3)(6.02 \times 10^{23}) / (104.1 \text{ g/mol}) = 6.02 \times 10^{21} \text{ cm}^{-3}$, and the infrared illuminated area of the sample is $S = (\pi/4)D^2 = (\pi/4)(0.1 \text{ cm})^2 = 7.85 \times 10^{-3} \text{ cm}^2$ [63].

Remarkably, the experimental result is in pleasing agreement with this prediction and provides confirmation of the axion-photon coupling strength [63]:

$$\sqrt{\frac{\alpha_{A\theta}(6)}{\alpha_{A\theta}(4)}} = \sqrt{\frac{(1.28 \pm 0.14) \text{ cm}^{-1}}{(15.9 \pm 0.7) \text{ cm}^{-1}}} = 0.284 \pm 0.017, \quad (4.9)$$

where we have used $T_{A\theta}(6) = (75.0 \pm 1.3)\%$ and $T_{A\theta}(4) = (12.1 \pm 1.0)\%$ from ref. [63]. We take this as striking confirmation of the predicted axion-photon coupling strength of 0.5 eV QCD axion dark matter given in Eq. (3.8). The experimental confirmation indicates that 0.5 eV QCD axion dark matter does indeed solve the so-called Strong CP problem of quantum chromodynamics [47–49].

4.5 Summary of 0.5 eV QCD Axion Dark Matter Rest-Mass Determination

In this section, the rest-mass energy of 0.5 eV QCD axion dark matter was determined experimentally to 44 parts per million precision:

$$m_A c^2(\text{Experiment}) = (0.50580 \pm 0.00002) \text{ eV}.$$

The determination confirms the percent-level precision prediction for the rest-mass energy given in the previous section:

$$m_A c^2(\text{Theory}) = (0.508 \pm 0.004) \text{ eV}. \quad (4.10)$$

Combining the experimental determination from this section with the cosmological argument from the previous section, we conclude that 0.5 eV QCD axion dark matter forms the dark matter in the universe. In the next section, we discuss the implications for cosmology and astroparticle physics that follow from our discovery of the particle nature of dark matter.

5 0.5 eV QCD Axion Dark Matter Implications

In the previous three sections, a model for the particle nature of 0.5 eV QCD axion dark matter was given, its rest-mass energy $m_A c^2 \approx 0.5$ eV was predicted assuming that it forms the dark matter in the universe, and an experimental confirmation of this prediction was presented. The clear implication is that 0.5 eV QCD axion dark matter indeed forms the dark matter in the universe. However, there are further implications for cosmology and astroparticle physics. This is the subject of the present section. In the introduction, we noted that the dark matter concept emerged from the tension between theoretical [2] and observational cosmology [1, 3]. However, it quickly spread to explain not just the spread in the redshifts of galaxies within clusters [4, 5, 10], but also the flat rotation curves of individual galaxies [6–10]. The further implication of our solution of the dark matter problem in astroparticle physics is that both the spread in the galaxy cluster redshifts and the flat rotation curves of galaxies are due to 0.5 eV QCD axion dark matter.

Following this implication, the energy density $\rho_A \approx 0.3 \text{ GeV/cm}^3$ of 0.5 eV QCD axion dark matter on Earth must match the best present astrophysical estimate of the energy density of dark matter in the local “halo” of the Milky Way [66]

$$\rho_{\text{DM}} = (0.30 \pm 0.03) \text{ GeV/cm}^3. \quad (5.1)$$

A direct determination of the 0.5 eV QCD axion dark matter energy density in a laboratory experiment $\rho_A \approx 0.3 \text{ GeV/cm}^3$ is then possible using the coupling of 0.5 eV QCD axion dark matter from the local dark matter ‘‘halo’’ of the galaxy to photons, to gluons, and to the neutral ρ^0 vector mesons that dominate photon-hadron interactions [67]. Such direct experimental determinations of ρ_A are the subjects of the rest of this section.

5.1 0.5 eV QCD Axion Dark Matter Shifts α

In the case of photons, the coupling to 0.5 eV QCD axion dark matter from the local dark matter halo shows up as a change in the effective value of the electromagnetic ‘‘fine-structure’’ constant α that governs quantum electrodynamic (QED) effects on charged leptons [68]. To leading order in $\alpha \approx 1/137$, QED effects — such as the shift $a_\ell = (g_\ell - 2)/2 \approx \alpha/(2\pi) = 1.164 \times 10^{-3}$ of the magnetic dipole moment of the charged lepton ℓ — come from an emergent mass term in the Dirac equation created by the proper electromagnetic radiation field of the charged lepton itself [69]. The axion-photon coupling in Eq. (3.7) changes the photon propagator that enters this emergent mass term.

Effectively, the change in the photon propagator can be absorbed into a change in the value of the fine-structure constant

$$\frac{\Delta\alpha}{\alpha} = g_{A\gamma\gamma} m_A c^2 \sqrt{\frac{\rho_A N_\ell V_\ell T_\ell}{\hbar}}, \quad (5.2)$$

where N_ℓ is the number of charged leptons ℓ interacting with the proper radiation field, V_ℓ is the luminous volume where this interaction takes place, and T_ℓ is the coherent life-time of the charged lepton within the luminous volume. Using $\rho_A = \rho_{\text{DM}} = (0.30 \pm 0.03) \text{ GeV/cm}^3$ for the local energy density of 0.5 eV QCD axion dark matter, we can predict the size of the resulting shift in the muon magnetic dipole moment measured with muon spin precession in magnetic storage rings

$$\Delta a_\mu = a_\mu \frac{\Delta\alpha}{\alpha} = (170 \pm 10) \times 10^{-11} \left(\frac{N_\mu}{2 \times 10^3} \right)^{1/2} \left(\frac{V_\mu}{3 \times 10^4 \text{ cm}^3} \right)^{1/2} \left(\frac{T_\mu}{64 \text{ } \mu\text{sec}} \right)^{1/2} \quad (5.3)$$

where N_μ is the number of muons whose spins are precessing within the magnetic storage ring, $V_\mu = 2\pi^2 \sigma_x \sigma_y R$ is the volume of the muon beam of width σ_x and height σ_y within the storage ring of radius R , and $T_\mu = \tau_\mu \sqrt{(p_\mu/(m_\mu c)^2 + 1)}$ is the life-time of the muon beam with momentum p_μ in the rest-frame of the ring for muon rest-mass $m_\mu = 105.7 \text{ MeV/c}^2$ [24] and rest-frame lifetime $\tau_\mu = 2.20 \text{ } \mu\text{sec}$ [24]. The predicted shifts are shown in Table 4 together with the input parameters for the three muon $g - 2$ experiments whose beam parameters are given in Table 5.

Remarkably, the size of the predicted shifts $\Delta a_\mu(\text{BNL}) = (167 \pm 10)^{-11}$ and $\Delta a_\mu(\text{FNAL}) = (171 \pm 10) \times 10^{-11}$ come out roughly the same for the Brookhaven (BNL E821) [70] and Fermilab (E989) [71] experiments. These experiments indeed obtained compatible results for a_μ within the 0.6 ppm precision of the comparison which is set mainly by the Brookhaven experiment $\sigma_{a_\mu}(\text{BNL}) = 63 \times 10^{-11}$. The predicted shift $\Delta a_\mu(\text{J-PARC}) = (50 \pm 3) \times 10^{-11}$ for the J-PARC experiment [72] is roughly the same size as the 0.5 ppm design precision $\sigma_{a_\mu}(\text{J-PARC}) = 60 \times 10^{-11}$.

In passing, we note that the single most precise present determination of the fine-structure constant α relies on the measurement of the magnetic dipole moment of the electron $a_e = (g_e - 2)/2 \approx \alpha/(2\pi) = 1.164 \times 10^{-3}$ to 110 parts per *trillion* precision with uncertainty

Experiment	N_μ (10^3)	V_μ (10^4 cm 3)	T_μ (usec)	Δa_μ (10^{-11})
BNL E821 [70]	1.29	4.51	64.4	167 ± 10
FNAL E989 [71]	1.93	3.12	64.4	171 ± 10
JPARC E34 [72]	10	0.49	6.6	50 ± 3

Table 4. 0.5 eV QCD Axion Dark Matter Shifts Muon $g-2$ —The number of muons N_μ stored within luminous volume V_μ with life-time T_μ for Brookhaven (BNL E821) [70], Fermilab (FNAL E989) [71], and J-PARC (JPARC E34) [72] muon spin precession experiments in magnetic storage rings with beam parameters in Table 5 yield a percent-level prediction for the shift $\Delta a_\mu = \Delta g_\mu/2 \approx \Delta\alpha/(2\pi)$ of the muon magnetic dipole moment $a_\mu = (g_\mu - 2)/2$ by 0.5 eV QCD axion dark matter from the local dark matter “halo” of the galaxy given by Eq. (5.3). J-PARC muon number is the design goal. Brookhaven and Fermilab muon numbers are measured values [73].

Experiment	σ_x (cm)	σ_y (cm)	R (cm)	p_μ (MeV/c)
BNL E821 [70]	1.78	1.25	711	3094
FNAL E989 [71]	2.10	1.53	711	3094
JPARC E34 [72]	1.5	5.0	33.3	318

Table 5. Muon Beam Parameters for 0.5 eV QCD Axion α Shift—Muon beam width σ_x and height σ_y in magnetic storage ring of radius R for muon momentum p_μ at Brookhaven (BNL E821) [70], Fermilab (FNAL E989) [71], and J-PARC (E34) [72] muon spin precession experiments. J-PARC width and height refer to the designed magnetic storage field region [72]. Brookhaven and Fermilab width and height are measured muon beam values [73].

$\sigma_{a_e} = 130 \times 10^{-15}$ [74]. The shift of the fine-structure constant $\Delta\alpha$ by 0.5 eV QCD axion dark matter given in Eq. (5.2) translates to a shift in the magnetic dipole moment in these experiments given by a formula analogous to the relation in Eq. (5.3) for the shift of the muon magnetic dipole moment Δa_μ measured by muon spin precession in magnetic storage rings:

$$\Delta a_e = a_e \frac{\Delta\alpha}{\alpha} = (0.90 \pm 0.06) \times 10^{-15} \left(\frac{N_e}{1} \right)^{1/2} \left(\frac{V_\mu}{4.0 \times 10^{-10} \text{ cm}^3} \right)^{1/2} \left(\frac{T_\mu}{2.7 \text{ sec}} \right)^{1/2}, \quad (5.4)$$

where $N_e = 1$ is the number of electrons — *usually just one* — trapped within the volume $V_e = 4\pi\rho_m\ell_B\sqrt{\langle z^2 \rangle} \approx (4.0 \times 10^{-10} \text{ cm}^3)(\rho_m/0.1 \text{ cm})$ traced out by a combination of three electron motions [74]: (1) Axial oscillation along a vertical magnetic field of strength $B = 5.3$ T with root-mean-square amplitude $\sqrt{\langle z^2 \rangle} = (1/2\pi\nu_z)\sqrt{kT_z/m_e} = (4.0 \pm 0.4) \times 10^{-4}$ cm at temperature $T_z = (0.55 \pm 0.11)$ K and frequency $\nu_z = 114$ MHz, (2) zero-point cyclotron motion with magnetic length $\ell_B = \sqrt{\hbar/(eB)} = 1.13 \times 10^{-6}$ cm, and (3) circular magnetron motion with radius $\rho_m \approx 0.1$ cm that is small compared with the 3 cm *outer* diameter of the microwave cavity where the electron is confined. Here, the coherence time $T_e = 1/(2\pi\Delta\nu_a)$ is set by the line-width $\Delta\nu_a = 0.06$ Hz of the combined spin-flip and cyclotron relaxation with frequency $\nu_a = a_e B/(2\pi m_e) = 173$ MHz from which a_e is determined [74]. The bottom line is that the predicted shift $\Delta a_e \approx 1 \times 10^{-15}$ from Eq. (5.4) is *more than 100 times smaller* than the current uncertainty of the measurement $\sigma_{a_e} = 130 \times 10^{-15}$.

5.2 0.5 eV QCD Axion Dark Matter Shifts α_s

In the case of the gluon, the coupling to 0.5 eV QCD axion dark matter from the local dark matter halo shows up as a change in the effective value of the “strong” coupling constant α_s

Experiment	Collider	Type	Q (GeV/c)	$\Delta\alpha_s(M_V)/\alpha_s(M_V) (10^{-4})$
CDF,D0	Tevatron Run 2	$p\bar{p}$	6.24 [77]	77 ± 4
ATLAS	LHC Run 1	pp	6.24 [77]	13.1 ± 0.6
CMS	LHC Run 2	pp	6.24 [77]	6.7 ± 0.3
JADE,TASSO	PETRA	$e\bar{e}$	35 [78]	-390 ± 17

Table 6. 0.5 eV QCD Axion Dark Matter Shifts α_s — Experiments at high-energy colliders of type proton-antiproton ($p\bar{p}$), proton-proton (pp) and electron-positron ($e\bar{e}$) with vector boson momentum Q in the lab frame. The predicted shift of the strong coupling constant due to the coupling of gluons to the 0.5 eV QCD axion dark matter from the local dark matter halo given by Eq. (5.6) is $\Delta\alpha_s(M_W)$ for W boson production from quark-antiquark annihilation during hadron collisions (pp and $p\bar{p}$). The shift is $\Delta\alpha_s(M_Z)$ for quark-antiquark dijet production from electron-positron annihilation ($e\bar{e}$).

that governs quantum chromodynamic (QCD) effects on quarks [75, 76]. The axion-gluon coupling takes the form [26–28, 49]

$$\mathcal{L}_{Ag} = g_{Agg}\phi_A \sum_{a=1}^8 \mathbf{E}^a \cdot \mathbf{B}^a, \quad (5.5)$$

where $g_{Agg}f_A = \alpha_s/(8\pi)$ gives the axion-gluon coupling strength, \mathbf{E}^a is the chromoelectric field, \mathbf{B}^a is the chromomagnetic field, and the index $a = 1, 2, \dots, 8$ runs over the eight gluons. The axion-gluon coupling shifts the gluon propagator that enters QCD effects such as (a) the average jet thrust $\langle d \rangle = 1/2 - 0.263(\alpha_s(Q)/\pi)$ [76] for a quark jet and an antiquark jet emerging from electron-positron annihilation with momentum transfer Q , and (b) the leading order QCD radiative correction $(4/3)(\alpha_s(M_W)/\pi) \log(M_Z^2/M_W^2)$ [75] to W boson production from quark-antiquark annihilation during hadron collisions with center-of-mass energy large compared to the rest-mass energy $M_W c^2 = 80.4$ GeV of the W boson and $M_Z c^2 = 91.2$ GeV of the Z boson [24].

Effectively, the shift of the gluon propagator can be absorbed in a change in the value of the strong coupling constant whose sign reflects the fact that the axion is odd $\mathcal{T}A_M = -A_M$ under time-reversal (See Sec. 2.3):

$$\begin{aligned} \frac{\Delta\alpha_s(M_W)}{\alpha_s(M_W)} &= g_{Agg}p_W c \sqrt{\rho_A V_{q\bar{q}} T_{q\bar{q}}/\hbar} \\ \frac{\Delta\alpha_s(M_Z)}{\alpha_s(M_Z)} &= -g_{Agg}Q c \sqrt{\rho_A V_{e\bar{e}} T_{e\bar{e}}/\hbar}, \end{aligned} \quad (5.6)$$

where the first line gives the change for W boson production $q\bar{q} \rightarrow V$ with $V = W^\pm$ and average momentum $p_W = 6.24$ GeV/c [77] from quark-antiquark annihilation during a hadron collision with luminous four-volume $V_{q\bar{q}} T_{q\bar{q}} = 16\pi\sigma_x\sigma_y\sigma_z^2/c$ created by the overlap in space and in time of the pair of hadron bunches with bunch width σ_x , height σ_y , and length σ_z . The second line gives the change for the *time-reversed* reaction $V \rightarrow q\bar{q}$ with $V = Z^0, \gamma$ in which a quark-antiquark dijet is produced with momentum transfer Q from electron-positron annihilation within the luminous four-volume $V_{e\bar{e}} T_{e\bar{e}}$ determined by the overlap in space and in time of the electron and positron bunches in the interaction region within the particle detector. Table 6 shows the resulting changes in the strong coupling constant for several high-energy particle physics experiments using the collider parameters collected in Table 7.

Collider	σ_x (μm)	σ_y (μm)	σ_z (cm)
Tevatron Run 2	22	22	47.5
LHC Run 1	18.8	18.8	9.4
LHC Run 2	9.3	9.3	9.7
PETRA	430	13	1.3

Table 7. Collider Parameters for 0.5 eV QCD Axion Dark Matter α_s Shift—Bunch width σ_x , height σ_y , and length σ_z for high-energy colliders entering predictions for the shifts of the strong coupling constant shown in Table 6. Tevatron and LHC parameters are from ref. [79] where we have taken the average of proton and antiproton parameters for the Tevatron. PETRA parameters are from ref. [80]

Determination	M_W (MeV/c 2)	ΔM_W (MeV/c 2)	$M_W - \Delta M_W$ (MeV/c 2)
Standard Model [84]	80,356 (5)	0	80,356 (5)(0)
ATLAS [85, 86]	80,367 (16)	13.3 (6)	80,354 (16)(0.6)
CDF [82]	80,433.5 (9.4)	78 (4)	80,355.5 (9.4)(4)
CMS [87]	80,360.2 (9.9)	6.8 (3)	80,353.4 (9.9)(0.3)

Table 8. 0.5 eV QCD Axion Dark Matter Shifts W Mass—Experimental determinations of the mass M_W of the charged W weak vector boson using quark-antiquark annihilation $q\bar{q} \rightarrow W$ during hadron collisions [82, 85–87] reveal the shift ΔM_W created by 0.5 eV QCD axion dark matter from the local dark matter halo of the galaxy given in Eq. (5.10) in terms of the shift $\Delta\alpha_s(M_W)$ of the strong coupling constant during the experiment (See Table 6 and the first line of Eq. (5.6)). Correcting for the shift, the W mass values determined from the experiments $M_W - \Delta M_W$ *agree with one another and with the prediction from the standard model of particle physics* given in the first line of the table (See Table 10.4 of ref. [84]) to within the precision of the comparison. In the last column, the first uncertainty is from the W mass determination itself and is uncorrelated between different determinations (Adds in quadrature). The second uncertainty is from ΔM_W and is fully correlated between the different determinations (Adds linearly).

Remarkably, both types of shifts of the strong coupling constant predicted in Eq. (5.6) appear to have already been observed [78, 82]. In 2011 Abbate *et al.* used the thrust of quark-antiquark dijets produced by electron-positron annihilation at the TASSO and JADE experiments to determine the strong coupling constant $\alpha_s(M_Z, \text{Thrust}) = 0.1135 \pm 0.0011$ [78]. However, the experimental determination differs by 3.6σ from the best present theoretical determination $\alpha_s(M_Z, \text{Lattice}) = (0.1182 \pm 0.0008)$ [83] based on lattice QCD:

$$\alpha_s(M_Z, \text{Thrust}) - \alpha_s(M_Z, \text{Lattice}) = -(47 \pm 13) \times 10^{-4}. \quad (5.7)$$

Both the sign and the size of the observed shift given in Eq. (5.7) agree with the predicted shift from Eq. (5.6) shown in Table 6 for the TASSO and JADE experiments:

$$\Delta\alpha_s(M_Z, \text{Thrust}) = \frac{\Delta\alpha_s(M_Z, \text{Thrust})}{\alpha_s(M_Z)} \alpha_s(M_Z, \text{Lattice}) = -(46 \pm 2) \times 10^{-4}. \quad (5.8)$$

We interpret the pleasing agreement between Eq. (5.7) and Eq. (5.8) to mean that 0.5 eV QCD axion dark matter indeed has the local energy density $\rho_A \approx 0.3 \text{ GeV/cm}^3$ suggested by the best present astrophysical estimates [66].

In April 2022 the CDF II collaboration reported the experimental determination $M_W(\text{CDF}) = (80,433.5 \pm 9.4) \text{ MeV/c}^2$ [82] of the W boson rest-mass from W boson production by quark-antiquark annihilation during proton-antiproton collisions. The experimental result differs by

seven standard deviations from the value predicted by the standard model of particle physics $M_W(\text{SM}) = (80, 356 \pm 5) \text{ MeV}/c^2$ (Table 10.4 in ref. [84]):

$$M_W(\text{CDF}) - M_W(\text{SM}) = (77 \pm 11) \text{ MeV}/c^2. \quad (5.9)$$

However, the predicted shift of the strong coupling constant by 0.5 eV QCD axion dark matter from the local dark matter halo given in Eq. (5.6) implies a corresponding shift of the W mass to keep fixed the leading QCD contribution to the quark-antiquark annihilation amplitude $(4/3)(\alpha_s(M_W)/\pi) \log(M_Z^2/M_W^2)$ [75]:

$$0 = \Delta\alpha_s(M_W) \log\left(\frac{M_Z}{M_W}\right) - \alpha_s(M_W) \frac{\Delta M_W}{M_W}. \quad (5.10)$$

Combining Eq. (5.10) with the shift of the strong coupling constant for the CDF experiment given in the top line of Table 6, we find the predicted shift of the W mass:

$$\begin{aligned} \Delta M_W(\text{CDF}) &= M_W \log\left(\frac{M_Z}{M_W}\right) \frac{\Delta\alpha_s(M_W)}{\alpha_s(M_W)} \\ &= (78 \pm 4) \text{ MeV}/c^2, \end{aligned} \quad (5.11)$$

Comparing the predicted shift in Eq. (5.11) with the observed shift in Eq. (5.9), we find a striking agreement. This agreement confirms that 0.5 eV QCD axion dark matter has local energy density $\rho_A \approx 0.30 \text{ GeV}/\text{cm}^3$ given by the best present astrophysical estimate of the local energy density of the dark matter halo of the galaxy [66].

In September 2024 the CMS collaboration reported the determination $M_W(\text{CMS}) = (80, 360.2 \pm 9.9) \text{ MeV}/c^2$ [87] from LHC Run 2 that differs by *five standard deviations* from the CDF determination:

$$M_W(\text{CDF}) - M_W(\text{CMS}) = (73 \pm 14) \text{ MeV}/c^2. \quad (5.12)$$

Yet, this difference in the W mass simply reflects — via Eq. (5.10) — the difference in the size of the strong coupling shifts at CMS during LHC Run 2 and at CDF during Tevatron Run 2 shown in Table 6:

$$\Delta M_W(\text{CDF}) - \Delta M_W(\text{CMS}) = (71 \pm 4) \text{ MeV}/c^2. \quad (5.13)$$

Comparing the observed shift in W mass between CDF and CMS in Eq. (5.12) and the predicted shift in Eq. (5.13), we again find pleasing agreement that confirms the consistency of the analysis. In Table 8, we summarize the analysis of the shift of the W mass by 0.5 eV QCD axion dark matter.

5.3 0.5 eV QCD Axion Dark Matter Shifts $a_\mu^{\pi\pi}$

In the case of the neutral ρ^0 vector mesons that dominate photon-hadron interactions [67], the coupling to 0.5 eV QCD axion dark matter from the local dark matter halo manifests as a shift in the leading order hadronic vacuum polarization contribution $a_\mu^{\pi\pi} \approx 3800 \times 10^{-11}$ [88] to the muon magnetic dipole moment from charged pion pair $\pi^+\pi^-$ production on the ρ^0 resonance. The axion-meson coupling takes the form:

$$\mathcal{L}_{A\rho} = g_{A\rho\omega} \phi_A \vec{\rho} \cdot \vec{\omega}, \quad (5.14)$$

Experiment	$a_\mu^{\pi\pi}(10^{-11})$	$\Delta a_\mu^{\pi\pi}(10^{-11})$	$a_\mu^{\pi\pi}(\text{SM})(10^{-11})$
CMD-3	3793 (30)	0	3793 (30)(0)
BABAR	3701 (27)	59 (3)	3760 (27)(3)
CMD-2	3665 (34)	76 (4)	3741 (34)(4)
BES-III	3618 (36)	62 (4)	3680 (36)(4)
KLOE	3606 (21)	179 (11)	3785 (21)(11)

Table 9. 0.5 eV QCD Axion Dark Matter Shifts $a_\mu^{\pi\pi}$ —Leading order hadronic contribution $a_\mu^{\pi\pi}$ to the muon magnetic dipole moment determined by pion pair production $\pi^+\pi^-(\gamma)$ from electron-positron annihilation with center-of-mass energy in the range $0.6 \leq \sqrt{s} \leq 0.88$ GeV at various experiments compiled by ref. [88]. The luminous four-volume created by the colliding electron and positron bunches produces the shift $\Delta a_\mu^{\pi\pi}$ given by Eq. (5.15). The Standard Model value $a_\mu^{\pi\pi}(\text{SM}) = a_\mu^{\pi\pi} + \Delta a_\mu$ corrects for the effect of 0.5 eV QCD axion dark matter and *agrees* between different experiments yielding a determination to 0.4% (See Eq. (5.16)).

where $\vec{\rho}$ is the vector field of the neutral ρ^0 vector meson, $\vec{\omega}$ is the vector field of the neutral ω vector meson [24], and $g_{A\rho\omega} = g_{A\gamma\gamma}g_\rho g_\omega/(4\pi\alpha) = 898$ $g_{A\gamma\gamma} = (611 \pm 18) \times 10^{-10}$ GeV $^{-1}$ [67] expresses the axion-meson coupling in terms of the axion-photon coupling $g_{A\gamma\gamma} = (0.68 \pm 0.02) \times 10^{-10}$ GeV $^{-1}$ (See Eq. 3.8) using the vector meson couplings $g_V = \alpha\sqrt{4\pi m_V/(3\Gamma_V^{ee})}$ [67] for $V = \rho^0, \omega$. Here, $m_\rho = 775$ MeV is the ρ^0 rest-mass energy, $m_\omega = 783$ MeV is the ω rest-mass energy, and the partial width Γ_V^{ee} gives the rate that V produces an electron-positron pair [24]: $\Gamma_\rho^{ee} = \Gamma_\rho \times \text{B.R.}(\rho \rightarrow e^+e^-) = (147 \text{ MeV})(4.72 \times 10^{-5}) = 6.94 \text{ keV}$ and $\Gamma_\omega^{ee} = \Gamma_\omega \times \text{B.R.}(\omega \rightarrow e^+e^-) = (8.68 \text{ MeV})(7.38 \times 10^{-5}) = 0.641 \text{ keV}$.

The coupling to 0.5 eV QCD axion dark matter from the local dark matter halo of the galaxy in Eq. (5.14) converts neutral ρ^0 vector mesons into ω vector mesons during measurements of charged pion $\pi^+\pi^-(\gamma)$ pair production from electron-positron annihilation [88]. The odd-parity ω vector meson decays mainly to three pions ($\pi^+\pi^-\pi^0$) [24] leading to a deficit in $a_\mu^{\pi\pi}$ compared to the standard model of particle physics:

$$\begin{aligned} \Delta a_\mu^{\pi\pi} &= g_{A\rho\omega} E_\rho \sqrt{\frac{\rho_A V_{e\bar{e}} T_{e\bar{e}}}{\hbar}} a_\mu^{\pi\pi} \\ &= (21.0 \pm 1.3) \times 10^{-11} \left(\frac{E_\rho}{1000 \text{ MeV}} \right) \left(\frac{\sigma_x}{100 \text{ }\mu\text{m}} \right)^{1/2} \left(\frac{\sigma_y}{10 \text{ }\mu\text{m}} \right)^{1/2} \left(\frac{\sigma_z}{1 \text{ cm}} \right), \end{aligned} \quad (5.15)$$

where E_ρ is the energy of the ρ^0 vector meson in the lab rest-frame, $V_{e\bar{e}} T_{e\bar{e}} = 16\pi\sigma_x\sigma_y\sigma_z^2/c$ gives the luminous four-volume created by colliding electron and positron bunches with width σ_x , height σ_y , and length σ_z .

We remark that — due to charge conservation — the axion-meson coupling cannot shift determinations of the leading order hadronic contribution $a_\mu^{\text{HLO}}(\rho^\pm)$ that are dominated by pion pair production $\pi^\pm\pi^0(\gamma)$ at the *charged* ρ^\pm vector meson resonance [89–92]. This reflects the fact that ω vector meson is isoscalar [24]. Unlike the isovector ρ meson, the ω has no charged counterparts into which the axion-meson coupling can convert the charged ρ^\pm vector mesons.

Table 9 shows five of the most precise determinations of $a_\mu^{\pi\pi}$ [88] together with the predicted shifts $\Delta a_\mu^{\pi\pi}$ from Eq. (5.15) using the beam parameters in Table 10 and Table 11 for all experiments except CMD-3. For CMD-3, the beam parameters reported in ref. [79] do not reflect the running conditions of the VEPP-2000 electron-positron collider during the measurements reported in ref. [88]. The actual bunch width, height, and length were significantly

Experiment	Collider	E (MeV)	E_ρ (MeV)
KLOE	DAΦNE	510	805
BES-III	BEPC-2	1885	1966
CMD-2	VEPP-2M	388	775
BABAR	PEP-II	5282	3131

Table 10. Beam Parameters for 0.5 eV QCD Axion Dark Matter $a_\mu^{\pi\pi}$ Shift I—Experiments at electron-positron colliders to detect $\pi^+\pi^-(\gamma)$ production from the neutral ρ^0 vector meson resonance at $m_\rho = 775$ MeV [24]. The beam has energy E and the ρ^0 meson has energy $E_\rho = \gamma\sqrt{p_\rho^2 + m_\rho^2} - \gamma\beta p_\rho$ in the lab frame. Here, $p_\rho = E - m_\rho^2/(4E)$ is the momentum of the ρ^0 meson in the center-of-mass frame. The time-dilation factor is $\gamma \approx 1.00$ and the speed is $\beta c \approx 0.00 c$ for the center-of-mass frame of the electron-positron collision with respect to the lab frame for all colliders except BABAR. For BABAR the effective beam energy $E = \sqrt{E_+ E_-} = 5282$ MeV is shown in the table, where, $E_+ = 3100$ MeV was the positron beam energy and $E_- = 9000$ MeV was the electron beam energy giving a time-dilation factor $\gamma = 1.15$ and speed $\beta c = 0.49 c$ [93]. The source for all beam parameters was Ref. [79] except VEPP-2M which came from Ref. [80].

Collider	σ_x (μm)	σ_y (μm)	σ_z (cm)
DAΦNE [81]	2000	20	3.0
DAΦNE [79]	260	4.8	2.0
BEPC-2 [79]	347	4.5	1.2
VEPP-2M [80]	400	10	3.0
VEPP-2M [80]	35	35	3.0
PEP-II [79]	157	4.7	1.05

Table 11. Beam Parameters for 0.5 eV QCD Axion Dark Matter $a_\mu^{\pi\pi}$ Shift II—Bunch width σ_x , height σ_y , and length σ_z refer to the size of the bunch at the interaction point within the detectors. For colliders with more than one set of beam parameters, the shift $\Delta a_\mu^{\pi\pi}$ was computed separately for each set of beam parameters using Eq. (5.15) and the equal-weight average of the shifts was then taken to give the results shown in the fourth column of Table 9.

smaller than the publicly reported values [94]. As a result, we simply took $\Delta a_\mu^{\pi\pi}(\text{CMD}) \approx 0$ to reflect the fact that actual shift is likely much smaller than the experimental uncertainty $\sigma_{a_\mu^{\pi\pi}}(\text{CMD}) = 30 \times 10^{-11}$.

The last column in Table 9 has the main result of this subsection. We have corrected the observed $a_\mu^{\pi\pi}$ for the shift $\Delta a_\mu^{\pi\pi}$ from axion-meson coupling. The result is five *compatible* determinations of the standard model value $a_\mu^{\pi\pi}(\text{SM})$. Combining these *compatible* determinations using the *experimental* uncertainties to fix the relative weight of each experiment in the combination, we find the standard model value to 0.4% precision:

$$a_\mu^{\pi\pi}(\text{SM}) = (3761 \pm 14) \times 10^{-11}, \quad (5.16)$$

where we have treated the shifts $\Delta a_\mu^{\pi\pi}$ as completely correlated and the experimental values $a_\mu^{\pi\pi}$ as completely independent.

Going further, we see a resolution of the 5.1σ tension $a_\mu^{\pi\pi}$ between the CMD-3 and KLOE experiments that was revealed in February 2023 [88]:

$$a_\mu^{\pi\pi}(\text{CMD3}) - a_\mu^{\pi\pi}(\text{KLOE}) = (187 \pm 37) \times 10^{-11}. \quad (5.17)$$

The resolution comes from comparing the observed tension in Eq. (5.17) with the predicted tension from Eq. (5.14):

$$\Delta a_\mu^{\pi\pi}(\text{KLOE}) - \Delta a_\mu^{\pi\pi}(\text{CMD3}) = (179 \pm 11) \times 10^{-11}. \quad (5.18)$$

Remarkably, we find pleasing agreement between the observed tension in Eq. (5.17) and the predicted tension Eq. (5.18). We take this pleasing agreement to provide support for the value of the local energy density $\rho_A \approx 0.3 \text{ GeV/cm}^3$ for 0.5 eV QCD axion dark matter that was used in the analysis and that saturates the local energy density of dark matter from astrophysical observations [66].

5.4 Comment on 0.5 eV QCD Axion Dark Matter Local Energy Density

In the previous three subsections, we analyzed the coupling of 0.5 eV QCD axion dark matter from the local dark matter halo to photons, to gluons, and to the neutral ρ^0 vector mesons that dominate photon-hadron interactions. By assuming that the local energy density $\rho_A \approx 0.3 \text{ GeV/cm}^3$ of 0.5 eV QCD axion dark matter saturates the best present astrophysical estimate of the local halo energy density $\rho_{\text{DM}} = (0.30 \pm 0.03) \text{ GeV/cm}^3$ [66], we found pleasing resolutions of several tensions and discrepancies in particle physics. The coupling to 0.5 eV QCD axion dark matter shifts the electromagnetic “fine-structure” constant α , the strong coupling constant α_s , and the leading order hadronic vacuum polarization contribution $a_\mu^{\pi\pi}$ to the muon magnetic dipole moment $a_\mu = (g_\mu - 2)/2$ from the ρ^0 resonance.

In this subsection, we take these tensions and discrepancies as experimental observations of the local energy density ρ_A of 0.5 eV QCD axion dark matter. By comparing the predicted shifts to the observed shifts, we then estimate ρ_A . In this way we make an *astroparticle* determination of the local halo energy density assuming that 0.5 eV QCD axion dark matter forms the dark matter in the local dark matter halo.

The most striking result in the previous subsections was the resolution of the *seven standard deviation discrepancy* in the W mass $M_W(\text{CDF}) - M_W(\text{SM}) = (77 \pm 11) \text{ MeV/c}^2$ in Eq. (5.9). If we now equate this to the predicted shift $\Delta M_W(\text{CDF}) = (78 \pm 4) \text{ MeV/c}^2$ in Eq. (5.11) using the collider parameters for the CDF experiment at Tevatron Run 2 in the predicted shift $\Delta\alpha_s$ of the strong coupling constant by 0.5 eV QCD axion dark matter in Eq. (5.6), then we obtain the following estimate for the local halo energy density of 0.5 eV QCD axion dark matter:

$$\rho_A(\text{CDF}) = (0.30 \text{ GeV/cm}^3) \left(\frac{M_W(\text{CDF}) - M_W(\text{SM})}{\Delta M_W(\text{CDF})} \right)^2 = (0.29 \pm 0.10) \text{ GeV/cm}^3, \quad (5.19)$$

where the uncertainty is dominated by that of the experimental tension. As expected, the experimental determination $\rho_A(\text{CDF}) \approx 0.30 \text{ GeV/cm}^3$ in Eq. (5.19) agrees with the best present astrophysical determination $\rho_{\text{DM}} = (0.30 \pm 0.03) \text{ GeV/cm}^3$ [66].

What is perhaps most noteworthy is that the *astroparticle* determination of the local dark matter halo energy density in Eq. (5.19) — which is the first of its kind — is already within a factor of three in precision of the best present astrophysical determination — assuming that 0.5 eV QCD axion dark matter form the dark matter in the local halo. The clear implication is that dedicated astroparticle determinations — as opposed to the serendipitous ones described in this section based on the analysis of past, current, and previously planned particle physics experiments — have the potential to directly probe the local dark matter energy density with comparable precision to the best present astrophysical observations. Perhaps an explanation

of the 13.7σ annual modulation in the single-hit, double-coincident scintillation event rate in thallium-doped sodium iodide reported by the DAMA/LIBRA astroparticle dark matter experiment [95, 96] could provide such a percent-level precision determination assuming that 0.5 eV QCD axion dark matter is responsible for the DAMA/LIBRA signal.

A hint in this direction is the $\Delta E = 0.41$ eV [97] activation energy that governs the room-temperature lifetime $\tau \approx 230$ nsec of the dark state of the excited thallium ion in sodium iodide. The relatively long dark state lifetime is used by the DAMA/LIBRA experiment to discriminate scintillation events from the relatively fast dark counts caused by double-coincident photomultiplier noise [95, 96]. The close coincidence of the scintillation activation energy $\Delta E = 0.41$ eV and the rest-mass energy $m_A c^2 \approx 0.5$ eV of 0.5 eV QCD axion dark matter suggests that axions may modulate the dark state scintillation lifetime $\tau \approx 230$ nsec to create the DAMA/LIBRA signal.

5.5 Summary of 0.5 eV QCD Axion Dark Matter Implications

In this section we discussed the implications for cosmology and astroparticle physics of our discovery of the particle nature of dark matter in the form of 0.5 eV QCD axions. The discovery supports the expanding universe cosmology by providing direct evidence for the existence of dark matter that can resolve the tension between the expanding universe cosmological redshift-distance relation and the significant scatter in the redshift of galaxies within galaxy clusters. In particular, dark matter in the form of 0.5 eV QCD axions has a cosmological energy density parameter that agrees within a percent with the dark matter energy density parameter estimated within the standard expanding universe cosmology [25].

Jumping from the cosmological to the astroparticle, we then discussed direct probes of the local energy density of 0.5 eV QCD axion dark matter in the local dark matter halo of the galaxy. The probes rely on the coupling of axions to photons, to gluons, and to the neutral ρ^0 vector mesons that dominate photon-hadron interactions. In all three cases, we found that certain particle physics experiments have sufficient precision and sensitivity to show the effects of coupling to 0.5 eV QCD axion dark matter from the local dark matter halo.

The analysis was organized in terms of the shift in fundamental constants caused by the coupling to axions. The shift in the electromagnetic “fine-structure” constant α was then analyzed in the context of measurements of the muon magnetic dipole moment $a_\mu = (g_\mu - 2)/2 \approx \alpha/(2\pi)$ using muon spin precession in magnetic storage rings in Section 5.1. The result showed that the two most precise measurements — at Brookhaven and at Fermilab — have roughly the same size shift Δa_μ . This result explains the rough agreement between the experimental results and predicts a significant tension with the standard model of particle physics.

The shift in the strong coupling constant α_s by 0.5 eV QCD axion dark matter from the local dark matter halo was discussed next in Section 5.2. Here, the most spectacular result was the resolution of the *seven standard deviation discrepancy* between the CDF collaboration’s experimental determination of the W mass and the value predicted within the standard model of particle physics. The analysis leading to the pleasing resolution of this large discrepancy — which far exceeds the conventional five standard deviation threshold for the discovery of a new phenomenon in experimental particle physics — was corroborated by a resolution along similar lines of the *five standard deviation discrepancy* between the CMS collaboration’s experimental W mass result and the CDF value.

Third, the shift of the leading order hadronic vacuum polarization contribution $a_\mu^{\pi\pi}$ to the muon magnetic dipole moment from the neutral ρ^0 vector meson was analyzed in terms

of the axion-meson coupling in Section 5.3. In this case, we were able to resolve a *five standard deviation discrepancy*. Here, the discrepancy that was resolved arose between the highest precision experimental determination of $a_\mu^{\pi\pi}$ (by the KLOE collaboration) and the most accurate such determination (by the CMD-3 collaboration).

Finally, a comment was made about the local energy density of 0.5 eV QCD axions in the dark matter halo in Section 5.4. Using the resolution of the *seven standard deviation* W mass discrepancy as a probe of this energy density, an *astroparticle* determination of the local halo energy density was made assuming that 0.5 eV QCD axions form the dark matter in the local halo and that their coupling to gluons is responsible for the W mass discrepancy. The result agrees with the best present astrophysical determination of the local halo energy density and is only three times less precise.

6 Conclusion

In this concluding section, we address several burning questions raised by our proposed solution of the dark matter problem in astroparticle physics. Perhaps the most pressing such question is the subject of the first subsection: How cold is 0.5 eV QCD axion dark matter? The standard expanding universe cosmology introduces an energy scale for answering this question. It comes from the redshift where the expansion history of the universe changes from being dominated by a light-like equation of state to being dominated by a matter-like equation of state.

We argue that 0.5 eV QCD axion dark matter in fact dominates the expansion of the universe on both sides of this epoch of so-called matter-radiation equality. In particular, the observational estimates of the energy-scale of the cross-over provide a direct cosmological probe of the rest-mass energy $m_{AC}c^2 \approx 0.5$ eV of the 0.5 eV QCD axion dark matter. A rough comparison indicates agreement between the observed expansion history of the universe up to “matter-radiation equality” and the history predicted by our proposed model for the particle nature of dark matter in terms of 0.5 eV QCD axion dark matter.

The next most burning question is addressed in the second subsection: How does the domination of the expansion history of the early universe by 0.5 eV QCD axion dark matter affect the synthesis of the nuclei of the light chemical elements? The precise mix of light elements that gets synthesized — mainly alpha particles with a smattering of deuterons — depends sensitively on the expansion history before Big Bang nucleosynthesis.

We argue that 0.5 eV QCD axion dark matter speeds up the expansion of the universe prior to Big Bang nucleosynthesis compared to the standard expanding universe cosmology [25]. That means more neutrons make it through the valley of death that begins with the “freeze-out” of weak nuclear reactions after the Big Bang and ends with the Big Bang nucleosynthesis of deuterons. By shortening the time of passage, 0.5 eV QCD axion dark matter ensures that more neutrons end up in light nuclei — for a given nucleon abundance — than in the standard expanding universe cosmology, we conclude.

In the last two subsections we tackle the burning astrophysical questions: How does 0.5 eV QCD axion dark matter cool the cores of horizontal branch stars in globular clusters, get the energy flow to reverse from the collapsing core of massive stars to power the neutrino flux observed from supernova SN 1987 A, and so on? These are tough questions to which we give a straightforward answer. Dark matter in the form of 0.5 eV QCD axions plays a critical role in the flow of energy within some old, dying, and dead stars (horizontal branch stars,

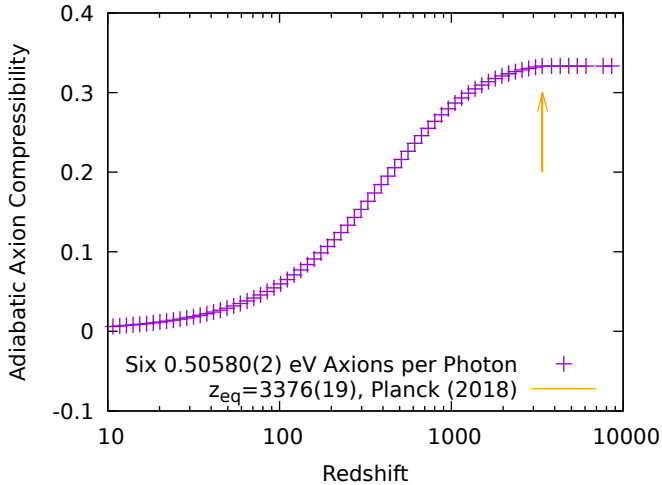


Figure 2. Cooling 0.5 eV QCD Axion Dark Matter—Adiabatic axion compressibility (purple crosses) in units of the axion energy density dp_A/du_A rises with increasing redshift for 0.5 eV QCD axion dark matter with rest-mass energy $m_A c^2 = (0.50580 \pm 0.00002)$ eV and number density $n_A/n_\gamma = 6$ that is six times that of photons in the cosmic background radiation. The compressibility saturates at the “light-like” value $dp_A/du_A \approx 0.333$ near the redshift $z_{\text{eq}} = 3376 \pm 19$ [25] (vertical orange arrow) that is interpreted as “matter-radiation equality” in the standard expanding universe cosmology.

core-collapse supernovae, and pulsars); however, it plays no role in the flow of energy within other such stars (white dwarfs and red giants).

6.1 How Cold is 0.5 eV QCD Axion Dark Matter?

In Section 3 we gave a cosmological argument for the rest-mass energy of 0.5 eV QCD axion dark matter. The conclusion of the argument was that 0.5 eV QCD axion dark matter forms the dark matter in the universe. But how cold is 0.5 eV QCD axion dark matter?

As part of the argument, we assumed that the present energy density of 0.5 eV QCD axion dark matter $u_A(T_\gamma) = n_A(T_\gamma)m_A c^2$ is simply the product of the present number density $n_A(T_\gamma)$ and the rest-mass energy $m_A c^2$. This is the defining relation of *cold* in the context of cosmology. It implies that the kinetic energy of 0.5 eV QCD axion dark matter is *small* compared to the $m_A c^2 \approx 0.5$ eV rest-mass energy.

But what happened right after the Big Bang at large redshift $z \approx T/T_\gamma$ when the temperature T was much greater than the present temperature $T_\gamma \approx 3$ K? Figure 2 shows the cooling curve for 0.5 eV QCD axion dark matter. The adiabatic compressibility dp_A/du_A in units of the axion dark matter energy density u_A — with p_A the pressure — starts at the “light-like” value $dp_A/du_A \approx 1/3$ for temperatures T much larger than the temperature $T_{\text{eq}} = z_{\text{eq}} T_\gamma \approx 10,000$ K set by the redshift $z_{\text{eq}} = 3376 \pm 19$ of “matter-radiation” equality in the standard expanding universe cosmology [25].

Then, as the universe expanded, the 0.5 eV QCD axion dark matter cooled. Right around the redshift $z_{\text{eq}} = 3376 \pm 19$ of “matter-radiation equality” in the standard expanding universe cosmology [25], the adiabatic compressibility rolls off to zero. This reflects the “matter-like” equation of state $p_A(z \ll z_{\text{eq}}) \approx n_A k T$. In contrast, above z_{eq} , the 0.5 eV QCD axion dark matter is better described by the “light-like” equation of state $p_A(z \gg z_{\text{eq}}) \approx (1/3)u_A$.

Importantly, the moment of “matter-radiation equality” is simply the point where the cooling 0.5 eV QCD axion dark matter begins to “feel” its rest-mass energy (Fig. 2). From the consistency of the observed value $z_{\text{eq}} = 3376 \pm 19$ [25] for this point and the predicted roll-off in the adiabatic compressibility shown in the figure, we conclude that our estimate $m_A c^2 \approx 0.5$ eV of the rest-mass energy of 0.5 eV QCD axion dark matter is on the right track. Conversely, given our direct determination of the axion rest-mass energy in Section 4, we conclude that the transition from “radiation-domination” to “matter-domination” within the standard expanding universe cosmology is in fact simply a change in the equation of state from “light-like” to “matter-like” for 0.5 eV QCD axion dark matter which dominates the expansion history of the universe on both sides of “matter-radiation equality.”

6.2 How Does 0.5 eV QCD Axion Dark Matter Effect Big Bang Nucleosynthesis?

The main effect of 0.5 eV QCD axion dark matter on Big Bang nucleosynthesis is shown in Fig. 3 ([18, 98], ref. [52], pg. 184–196). In the standard expanding universe cosmology, there are two key moments in the early universe’s expansion history that are critical to the efficiency of converting nucleons — neutrons n and protons p — into the nuclei of the light chemical elements — primarily alpha particles α with a tiny bit of deuterons d . The domination of the early expansion history of the universe by 0.5 eV QCD axion dark matter shrinks the gap in time between these two key moments compared to the standard expanding universe cosmology resulting in a significant increase in α production for a given amount of nucleons.

The first key moment in the early universe relevant for Big Bang nucleosynthesis occurs at the temperature $T_{n/p} \approx 10^{10}$ K when the ratio n/p stops tracking the thermal equilibrium value $\exp(-Q/kT)$ set by the difference $Q = m_n c^2 - m_p c^2 = 1.2933$ MeV [24] between the neutron and proton rest-mass energies. In the standard expanding universe cosmology, this temperature arrives at a time $t_{n/p} \approx 1$ sec after the Bang (ref. [52], pg. 185, Table 6.2). This value for $t_{n/p}$ does not significantly change when the early expansion history is dominated by 0.5 eV QCD axion dark matter moving with nearly the speed of light and having number density six times that of photons (Fig. 3).

Instead, the major change in the expansion history relevant to Big Bang nucleosynthesis is in the timing of the second key moment. It occurs at the temperature $T_d \approx 10^9$ K when the thermal equilibrium begins to favor radiative neutron capture $n + p \rightarrow d + \gamma$ over deuteron photo-disintegration $d + \gamma \rightarrow n + p$ due to the binding energy $B = m_p c^2 + m_n c^2 - m_d c^2 = 2.225$ MeV [24] of the deuteron beginning to far exceed the energy of the photons γ . In the standard expanding universe cosmology, this temperature arrives at at time $t_d \approx 200$ sec after the Big Bang (ref. [52], pg. 185, Table 6.2). The time delay after the Bang for this second key moment to occur is roughly half as large $t_d \approx 100$ sec when 0.5 eV QCD axion dark matter instead dominate the expansion history of the early universe (Fig. 3).

The rule of thumb in discussions of Big Bang nucleosynthesis is that you get one α particle for every pair of neutrons n which make it to the point in time t_d after the Bang when radiative neutron capture wins over deuteron photo-disintegration ([52], pg. 194). In other words, the network of fusion reactions which builds up α particles from the nucleons — n and p — makes sure that just about every neutron n makes it into an α particle (which consists of a pair of neutrons n and a pair of protons p). However, the neutrons must first survive the “valley of death” between the loss of thermal equilibrium in the relative abundance n/p of neutrons and protons at time $t_{n/p} \approx 1$ sec and the beginning of Big Bang nucleosynthesis at t_d . By significantly cutting the time t_d , roughly by a factor of two, 0.5 eV QCD axion dark

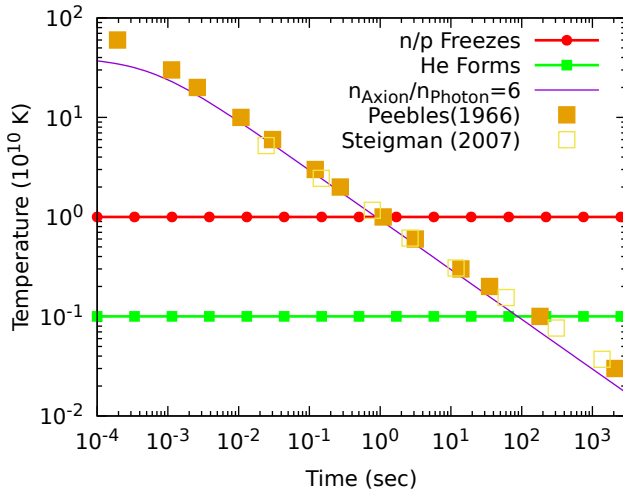


Figure 3. 0.5 eV QCD Axion Dark Matter Cools Universe Faster— The temperature of the universe ($n_{\text{Axion}}/n_{\text{Photon}} = 6$, diagonal purple line) cools with the time elapsed since the Big Bang due mainly to the energy density of 0.5 eV QCD axion dark matter moving with the speed of light and having number density *six times* that of photons. The cooling rate cuts the neutron decay time between the “freeze-out” of weak nuclear reactions at temperature $\sim 10^{10}$ K (n/p freezes, red horizontal line with dots) and the onset of Big Bang nucleosynthesis at temperature $\sim 10^9$ K (He forms, green horizontal line with boxes) when compared with the standard expanding universe cosmology from both the original calculation (Peebles (1966), filled gold boxes) [18] and also from the relatively recent review (Steigman (2007), open gold squares) [98].

matter significantly increases the number of neutrons n that make it to t_d and thence into α particles during Big Bang nucleosynthesis.

6.3 How Does 0.5 eV QCD Axion Dark Matter Mess with Stars?

The main way that 0.5 eV QCD axion dark matter messes with old, dying, and dead stars is that it cools them faster than standard astrophysical simulations would predict (Fig. 4). The oldest stars in the galaxy are the so-called Population II stars in the globular clusters that form a roughly spherical “halo” around the galactic center. A critical event in the development of the expanding universe cosmology in the mid-20th century was the recognition that the “metallicity” of these old stars — meaning the concentration of atomic nuclei which are *heavier* than protons and α particles — is significantly *lower* than the metallicity of relatively young stars, such as the Sun, that are found in the spiral arms of the galaxy [10].

Nevertheless, when the effect of the axion-photon coupling in Eq. (3.7) with the strength predicted in Eq. (3.8) is plugged into simulations of the evolution of globular cluster stars that are now burning α particles in their core through the reactions $\alpha + \alpha \rightarrow {}_4^8\text{Be} + \gamma$ and $\alpha + {}_4^8\text{Be} \rightarrow {}_6^{12}\text{C} + 2\gamma$, one finds that these so-called horizontal branch stars had *roughly the same core helium mass fraction when they formed* right after the Bang $Y_{\text{HB}} = 0.272 \pm 0.005$ [99] as the Sun had $Y_{\odot} = 0.274 \pm 0.005$ [100, 101] when it formed much later. The physical meaning of this result is that the production of 0.5 eV QCD axion dark matter in the core of these old stars *significantly* cools the α -burning core.

We conclude that there were *significantly more* α particles in the core of horizontal branch stars in globular clusters at formation right after the Big Bang than is predicted from Big Bang nucleosynthesis within the standard expanding universe cosmology $Y_{\text{BBN}} = 0.24709 \pm 0.00017$

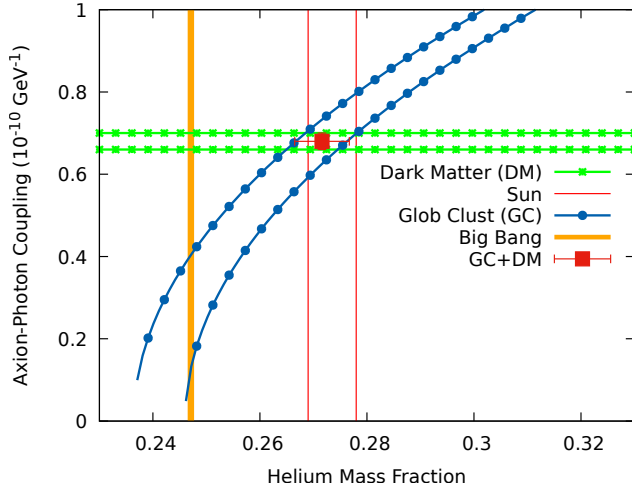


Figure 4. 0.5 eV QCD Axion Dark Matter Implies More Big Bang Helium—Simulations of helium burning in the core of horizontal branch stars in globular cluster (Glob Clust (GC), curved blue lines with dots) [99] imply *significantly more* helium was in the core of these stars when they formed shortly after the Big Bang (GC+DM, filled red square with error bars) than the “primordial” helium abundance predicted in the standard expanding universe cosmology (Big Bang, vertical gold band) [102] if the effect of axion-photon coupling is included in the simulation with the value of the coupling strength $g_{A\gamma\gamma} = (0.68 \pm 0.02) \times 10^{-10} \text{ GeV}^{-1}$ (Dark Matter (DM), horizontal green lines with boxes) predicted for 0.5 eV QCD axion dark matter (See Eq. 3.8). For comparison, we show the helium mass fraction in the core of the Sun when it formed (Sun, vertical red lines) [100, 101]. Although the Sun formed much later than the stars that are now on the horizontal branch of the temperature-luminosity diagram of globular clusters, the core helium mass fraction at formation surprisingly agrees within the percent-level precision of the comparison. This agreement indicates that there was *no significant* chemical evolution in the initial helium mass fraction in the cores of stars at their time of formation during *most* of the lifetime of the Milky Way.

[102]. This conclusion is in accord with the conclusion presented in the previous subsection on the basis of the domination of the expansion history of the early universe by 0.5 eV QCD axion dark matter. There we found that 0.5 eV QCD axion dark matter significantly speeds up the cooling of the universe leading to *significantly more* α particles coming out of Big Bang nucleosynthesis than in the standard expanding universe cosmology. Here we find a *five standard deviation* effect $Y_{\text{HB}} - Y_{\text{BBN}} = 0.025 \pm 0.005$.

6.4 Comment on White Dwarfs, Red Giants, Pulsars, and Supernova 1987A

The strength of the coupling g_{Aee} of 0.5 eV QCD axion dark matter to electrons appears to be precisely zero $g_{Aee} = 0$ based on analysis of the *unobserved* effects that such an axion-electron coupling would have on the cooling of white dwarfs and red giants were the strength g_{Aee} not precisely zero [28]. By contrast, the cooling of pulsars and the energy flow in the collapsing core of the progenitor star for supernova 1987 A *appear to both be dominated* by the effects of the *non-zero* axion-nucleon coupling to 0.5 eV QCD axion dark matter [28]. Indeed, the strength of the axion-nucleon coupling $g_{ANN}f_A \approx g_{\pi NN}f_\pi$ [49] is roughly set by the axion decay constant f_A in Eq. (3.2) and by the product $g_{\pi NN}f_\pi \approx g_A m_N c^2$ [24] of the pion-nucleon coupling strength $g_{\pi NN}$ with the pion decay constant f_π , where $g_A = -1.2754 \pm 0.0013$ [24] is the axial weak nuclear coupling strength and $m_N \approx 940 \text{ MeV}/c^2$ is the nucleon rest-mass.

6.5 Summary of 0.5 eV QCD Axion Dark Matter Conclusions

In summary, we have addressed several burning questions in cosmology and astroparticle physics that are raised by our proposed solution to the dark matter problem in astroparticle physics in the form of 0.5 eV QCD axion dark matter within an expanding universe cosmology. The equation of state of 0.5 eV QCD axion dark matter changes from “light-like” to “matter-like” in the early universe and this changes the expansion history from “radiation-dominated” to “matter-dominated” (See section 6.1). The domination of the early expansion history of the universe by 0.5 eV QCD axion dark matter — moving with nearly the speed of light and having number density *six times* that of photons — kick starts Big Bang nucleosynthesis about 100 seconds after the Bang (See section 6.2).

The resulting “primordial” helium abundance extracted from observations of some of the oldest stars in the galaxy — using stellar evolution codes that include the effects of axion-photon coupling with the strength predicted for 0.5 eV QCD axion dark matter — agrees with the best present estimates of the core helium abundance in the Sun at its time of formation *long after the Bang* (Section 6.3). This agreement suggests that *no significant* chemical evolution took place in the *core helium* abundance of stars *at their times of formation* during the life of the galaxy despite the well-known differences in the *metallicity* observed in stellar *atmospheres* [10] and the obvious chemical evolution in the core *after star formation*. Finally, we closed with a comment on the importance of 0.5 eV QCD axion dark matter to the flow of energy in pulsars and in core-collapse supernovae, and with a remark that 0.5 eV QCD axions *do not* seem to couple to electrons (Section 6.4).

Acknowledgments

The author acknowledges the critical and constant support of Daria Mazura.

References

- [1] F. Zwicky, *The Redshift of Extragalactic Nebulae*, *Helv. Phys. Acta* **6** (1933) pg. 110 in German. English and Spanish translation by H. Andernach, arXiv:1711.01693 (2017).
- [2] G. Lemaitre, *A Homogeneous Universe of Constant Mass and Growing Radius Accounting for the Radial Velocity of Extragalactic Nebulae*, *Annales Soc. Sci. Bruxelles A* **47** (1927) pg. 49 in French. English translation in *Gen. Rel. Grav.* **45** (2013) pg. 1635.
- [3] E. Hubble and M. L. Humason, *The Velocity-Distance Relation among Extra-Galactic Nebulae*, *Astrophys. J.* **74** (1931) pg. 43.
- [4] F. Zwicky, *On the Masses of Nebulae and of Clusters of Nebulae*, *Astrophys. J.* **86** (1937) pg. 217.
- [5] S. Smith, *The Mass of the Virgo Cluster*, *Astrophys. J.* **83** (1936) pg. 23.
- [6] H. Babcock, *The Rotation of the Andromeda Nebula*, *Lick Observatory Bulletin* **19** (1939) pg. 41.
- [7] H. Oort, *Some Problems Concerning the Structure and Dynamics of the Galactic System and the Elliptical Nebulae NGC 3115 and 44941*, *Astrophys. J.* **91** (1940) pg. 273.
- [8] A. B. Wyse and N. Mayall, *Distribution of Mass in the Spiral Nebulae Messier 31 and Messier 33*, *Astrophys. J.* **95** (1942) pg. 24.
- [9] N. Mayall, *Pubs. Obs. Univ. Michigan* **10** (1950) pg. 19.

- [10] M. Schwarzschild, *Mass Distribution and Mass-Luminosity Ratio in Galaxies*, *Astronom. J.* **59** (1954) pg. 273.
- [11] K. K. Kwee, C. Muller, and G. Westerhout, *Bull. Astron. Inst. Neth.* **12** (1954) pg. 1954.
- [12] H. C. van der Hulst, E. Raimond, and H. v. Woerden, *Bull. Astron. Inst. Neth.* **14** (1957) pg. 1.
- [13] J. Neyman, T. Page, and E. Scott, *Summary of the Conference*, *Astron. J.* **66** (1961) pg. 633.
- [14] V. C. Rubin, J. Burley, A. Kiasatpoor, B. Klock, G. Pease, E. Rutscheidt, and C. Smith, *Astron. J.* **67** (1962) pg. 491.
- [15] V. C. Rubin and J. Burley, *Kinematic Studies of Early-Type Stars. II The Velocity Field within 2 kpc of the Sun*, *Astron. J.* **69** (1964) pg. 80.
- [16] A. Penzias and R. W. Wilson, *A Measurement of Excess Antenna Temperature at 4080 Mc/s*, *Astrophys. J.* **142** (1965) pg. 419.
- [17] R. H. Dicke, P. J. E. Peebles, P. G. Roll, and D. T. Wilkinson, *Cosmic Black-Body Radiation*, *Astrophys. J.* **142** (1965) pg. 414.
- [18] P. J. E. Peebles, *Primordial Helium Abundance and the Primordial Fireball. II*, *Astrophys. J.* **146** (1966) pg. 542.
- [19] J. B. Rogerson and D. G. York, *Interstellar Deuterium Abundance in the Direction of Beta Centauri*, *Astrophys. J.* **186** (1974) pg. L95.
- [20] P. Hut, *Limits on masses and number of neutral weakly interacting particles*, *Phys. Lett. B* **69** (1977) pg. 85.
- [21] B. W. Lee and S. Weinberg, *Cosmological Lower Bound on Heavy-Neutrino Masses*, *Phys. Rev. Lett.* **39** (1977) pg. 165.
- [22] K. Sato and M. Kobayashi, *Cosmological Constraints on the Mass and the Number of Heavy Lepton Neutrinos*, *Prog. Theor. Phys.* **58** (1977) pg. 1775.
- [23] M. Vysotsky, A. Dolgov, and Y. Zeldovich, *Cosmological limits on the masses of the neutral leptons*, *JETP Lett.* **26** (1977) pg. 188.
- [24] S. Navas *et al.* [Particle Data Group], *Review of particle physics*, *Phys. Rev. D* **110** (2024) pg. 030001.
- [25] N. Aghanim, Y. Akrami, M. Ashdown, J. Aumont, C. Baccigalupi *et al.* (Planck Collaboration), *Planck 2018 Results VI. Cosmological Parameters*, *Astron. and Astrophys.* **641** (2018) pg. A6. *Planck 2018 Results: Cosmological Parameter Tables 68% Confidence Intervals* (May 14, 2019), pg. 49. “Baseline Λ CDM analysis 2.40.”
- [26] S. Weinberg, *A New Light Boson?*, *Phys. Rev. Lett.* **40** (1978) pg. 223.
- [27] F. Wilczek, *Problem of Strong P and T Invariance in the Presence of Instantons*, *Phys. Rev. Lett.* **40** (1978) pg. 279.
- [28] L. J. Rosenberg, G. Rybka and B. Safdi, *90. Axions and Other Similar Particles* in Ref. [24].
- [29] E. C. G. Sudarshan and R. E. Marshak, *Chiral Invariance and the Universal Fermi Interaction*, *Phys. Rev.* **109** (1958) pg. 1861.
- [30] R. P. Feynman and M. Gell-Mann, *Theory of the Fermi Interaction*, *Phys. Rev.* **109** (1957) pg. 193.
- [31] Z. Koba and S. Tomonaga, *Application of the “Self-Consistent” Subtraction Method to the Elastic Scattering of the Electron*, *Prog. Theor. Phys.* **2** (1947) pg. 218.
- [32] Z. Koba and S. Tomonaga, *On Radiative Reactions in Collision Processes. I*, *Prog. Theor. Phys.* **3** (1948) pg. 1648.

[33] J. Schwinger, *On Quantum-Electrodynamics and the Magnetic Moment of the Electron*, *Phys. Rev.* **73** (1948) pg. 416.

[34] J. Schwinger, *Quantum Electrodynamics. I. A Covariant Formulation*, *Phys. Rev.* **74** (1948) pg. 1439.

[35] J. Schwinger, *Quantum Electrodynamics. II. Vacuum Polarization and Self-Energy*, *Phys. Rev.* **75** (1949) pg. 651.

[36] J. Schwinger, *Quantum Electrodynamics. III. The Electromagnetic Properties of the Electron—Radiative Corrections to Scattering*, *Phys. Rev.* **76** (1949) pg. 790.

[37] R. P. Feynman, *Space-Time Approach to Quantum Electrodynamics*, *Phys. Rev.* **76** (1949) pg. 769.

[38] H. D. Politzer, *Reliable Perturbative Results for Strong Interactions?*, *Phys. Rev. Lett.* **30** (1973) pg. 1346.

[39] D. Gross and F. Wilczek, *Ultraviolet Behavior of Non-Abelian Gauge Theories*, *Phys. Rev. Lett.* **30** (1973) pg. 1343.

[40] S. Glashow, *Partial-symmetries of weak interactions*, *Nucl. Phys.* **22** (1961) pg. 579.

[41] S. Weinberg, *A Model for Leptons*, *Phys. Rev. Lett.* **19** (1967) pg. 1264.

[42] A. Salam, *Weak and Electromagnetic Interactions*, *Conf. Proc. C* **680519** (1968) pg. 367.

[43] See *Tests of Discrete Space-Time Symmetries: \mathcal{CPT} Invariance* in ref. [24].

[44] G. 't Hooft, *Symmetry Breaking through Bell-Jackiw Anomalies*, *Phys. Rev. Lett.* **37** (1976) pg. 8.

[45] G. 't Hooft, *Computation of the quantum effects due to a four-dimensional pseudoparticle*, *Phys. Rev. D* **14** (1976) pg. 3432.

[46] A. A. Belavin, A. M. Polyakov, A. S. Schwartz and Yu. S. Tyupkin, *Pseudoparticle Solutions of the Yang-Mills Equations*, *Phys. Lett. B* **59** (1975) pg. 85.

[47] R. D. Peccei and H. R. Quinn, *CP Conservation in the Presence of Pseudoparticles*, *Phys. Rev. Lett.* **38** (1977) pg. 1440.

[48] R. D. Peccei and H. R. Quinn, *Constraints imposed by CP conservation in the presence of pseudoparticles*, *Phys. Rev. D* **16** (1977) pg. 1791.

[49] R. D. Peccei, *Strong CP Problem*, *Adv. Ser. Direct. High Energy Phys.* **3** (1989) pg. 503.

[50] M. Gorgetto and G. Villadoro, *Topological susceptibility and QCD axion mass*, *JHEP* **2019** (2019) pg. 33.

[51] M. Benedikt *et al.*, *Future Circular Collider Study. Volume 3: The Hadron Collider (FCC-hh) Conceptual Design Report*, *Eur. Phys. J. ST* **228** (2019) pg. 755.

[52] P. J. E. Peebles, *Principles of Physical Cosmology*, Princeton University Press, Princeton, NJ (1992).

[53] D. J. Fixsen, *The Temperature of the Cosmic Microwave Background*, *Astrophys. J.* **707** (2009) pg. 916.

[54] Z. Fodor, C. Hoelbling, S. Krieg, L. Lellouch, T. Lippert, A. Portelli, A. Sastre, K. K. Szabao, and L. Varnhorst, *Up and Down Quark Masses and Corrections to Dashen's Theorem from Lattice QCD and Quenched QED*, *Phys. Rev. Lett.* **117** (2016) pg. 082001.

[55] M. Tasumi, *Introduction to Infrared Spectroscopy* in ref. [103], pgs. 3–14.

[56] C. Kittel, *Introduction to Solid State Physics*, 8th ed., Wiley, New York, NY (2005), pgs. 95–98.

[57] Polystyrene calibration thin film, 38 microns thick, International Crystal Laboratories, Garfield, NJ.

[58] D. Gupta, L. Wang, L. M. Hanssen, J. J. Hsia, and R. V. Datla, *Standard Reference Materials: Polystyrene Films for Calibrating the Wavelength Scale of Infrared Spectrometers SRM 1921; NIST Special Publication 260-122*, U.S. Government Printing Office: Washington, D.C. (1995).

[59] E. K. Plyer and C. W. Wilbur, *Wavelengths for Calibration of Prism Spectrometers*, *J. Res. Natl. Bur. Res. Stand.* **45** (1950) pg. 462.

[60] E. K. Plyer, A. Danti, L. R. Blaine, and E. D. Tidwell, *Vibration-Rotation Structure in Absorption Bands for the Calibration of Spectrometers from 2 to 16 Microns*, *J. Res. Natl. Bur. Res. Stand.* **64** (1960) pg. 29.

[61] W. Brugel, *An Introduction to Infrared Spectroscopy*, A. R. Karitsky and A. J. D. Karitsky trans. (Wiley, New York, NY 1962), pg. 353.

[62] NIST Standard Reference Material 1921(b), *Infrared Transmission Standard Wavelength/Wavenumber Standard*, Issued: 01 August 2023.

[63] S. R. Lowry, J. Hyatt, and W. J. McCarthy, *Determination of Wavelength Accuracy in the Near-Infrared Spectral region Based on NIST's Infrared Transmission Wavelength Standard SRM 1921*, *Appl. Spectrosc.* **54** (2000) pg. 450.

[64] J. R. Birch, *The Far-Infrared Optical Constants of Polypropylene, PTFE, and Polystyrene*, *Infrared Phys.* **33** (1992) pg. 33.

[65] M. Takayanagi, *Near Infrared Spectroscopy* in ref. [103].

[66] A.-C. Eilers et al, *The Circular Velocity Curve of the Milky Way from 5 to 25 kpc*, *Astrophys. J.* **871** (2019) pg. 120.

[67] R. P. Feynman, *Photon-Hadron Interactions* (Perseus, 1972), pp. 82–85, 96–97.

[68] J. Schwinger, *On Quantum-Electrodynamics and the Magnetic Moment of the Electron*, *Phys. Rev.* **73** (1948) pg. 416.

[69] J. Schwinger, *On Gauge Invariance and Vacuum Polarization*, *Phys. Rev.* **82** (1951) pg. 664, Appendix B.

[70] G.W. Bennett et al. (Muon $g - 2$), *Final report of the muon E821 anomalous magnetic moment measurement at BNL*, *Phys. Rev. D* **73** (2006) pg. 072003.

[71] D. P. Aguillard et al. (Muon $g - 2$), *Phys. Rev. D* **110** (2024) pg. 032009.

[72] M. Abe et al., *A new approach for measuring the muon anomalous magnetic moment and electric dipole moment*, *Prog. Theor. Part. Phys.* **2019** (2019) pg. 053C02.

[73] J. Mott, private communication.

[74] X. Fan, T. G. Myers, B. A. D. Sukra, and G. Gabrielse, *Measurement of the Electron Magnetic Moment*, *Phys. Rev. Lett.* **130** (2023) pg. 071801.

[75] H. Georgi and H. D. Politzer, *Electroproduction scaling in an asymptotically free theory of strong interactions*, *Phys. Rev. D* **9** (1974) pg. 416.

[76] E. Farhi, *Quantum Chromodynamics Tests for Jets*, *Phys. Rev. Lett.* **39** (1977) pg. 1587.

[77] F. Abe et al. (CDF Collaboration), *Measurement of the W Boson Mass*, *Phys. Rev. D* **52** (1995) pg. 4784.

[78] R. Abbate, M. Fickinger, A. H. Hoang, V. Mateu, and I. W. Stewart, *Thrust at N³LL with Power Corrections and a Precision Global Fit for $\alpha_s(m_Z)$* , *Phys. Rev. D* **83** (2011) pg. 074021.

[79] E. Pianori, *32. High Energy Collider Parameters*, in ref. [24].

[80] L. Montanet, K. Giesemann, R. M. Barnett, D. E. Groom, T. G. Trippe, C. G. Wohl et al. (Particle Data Group), *Review of particle properties*, *Phys. Rev. D* **50** (1994) pg. 1173, Section 13 High-Energy Collider Parameters: e^+e^- Colliders (III).

[81] F. Ambrosino *et al.* (KLOE Collaboration), *Beam parameters from first year at DAΦNE*, *Eur. J. Phys. C* **47** (2006) pg. 589.

[82] T. Aaltonen *et al.* (CDF Collaboration), *High-precision measurement of the W boson mass with the CDF II detector*, *Science* **376** (2022) pg. 170.

[83] S. Aoki *et al.* (FLAG Collaboration), *FLAG 2019 Review*, *Eur. Phys. J. C* **80** (2020) pg. 113.

[84] J. Erler and A. Freitas, *Section 10: Electroweak Model and Constraints on New Physics*, in ref. [24].

[85] M. Aaboud *et al.* (ATLAS Collaboration), *Measurement of the W -boson mass in pp collisions at $\sqrt{s} = 7$ TeV with the ATLAS detector*, *Eur. J. Phys. C* **78** (2018) pg. 110.

[86] M. Aadboud *et al.* (ATLAS), *Improved W Boson Mass Measurement using $\sqrt{s} = 7$ TeV Proton-Proton Collisions with the ATLAS Detector*, arXiv:2403.15085 (2024).

[87] CMS collaboration, *Measurement of the W boson mass in proton-proton collisions at $\sqrt{s} = 13$ TeV*, CMS PAS SMP-23-002 (2024).

[88] F. V. Ignatov *et al.* (CMD-3), *Measurement of the $e^+e^- \rightarrow \pi^+\pi^-$ cross section from threshold to 1.2 GeV with the CMD-3 detector*, *Phys. Rev. D* **109** (2024) pg. 112002.

[89] M. Fujikawa *et al.* (BELLE), *High-statistics study of the $\tau^- \rightarrow \pi^-\pi^0\nu_\tau$ decay*, *Phys. Rev. D* **78** (2008) pg. 072006.

[90] S. Schael *et al.* (ALEPH), *Branching ratio and structure functions of τ decays: Final ALEPH measurements and physics implications*, *Phys. Rept.* **421** (2005) pg. 191.

[91] M. Davier, A. Hoecker, B. Malaescu, C.-Z. Yuan, and Z. Zhang, *Update of the ALEPH non-strange spectral functions from hadronic τ decays*, *Eur. Phys. J. C* **74** (2014) pg. 2803.

[92] M. Davier, A. Hoecker, B. Malaescu, and Z. Zhang, *A new evaluation of the hadronic vacuum polarisation contributions to the muon anomalous magnetic moment and to $\alpha(m_Z^2)$* , *Eur. Phys. J. C* **80** (2020) pg. 241, [Erratum: *Eur. Phys. J. C* **80** (2020) pg. 410].

[93] A. J. Bevan, B. Golob, Th. Mannel, S. Prell, and B. D. Yabsley, *The Physics of the B Factories*, *Eur. Phys. J. C* **74** (2014) pg. 3026.

[94] Private communication, I. Logashenko and F. Ignatov.

[95] R. Bernabei *et al.* (DAMA/LIBRA), *Further results from DAMA/LIBRA-phase 2 and perspectives*, *Nucl. Phys. At. Energy* **22** (2021) pg. 329.

[96] R. Bernabei *et al.* (DAMA/LIBRA), *First model independent results from DAMA/LIBRA-phase 2*, *Nucl. Phys. At. Energy* **19** (2021) pg. 307.

[97] J. B. Birks, *Theory and Practice of Scintillation Counting*, Pergamon, London, UK (1964) pgs. 433-435.

[98] G. Steigman, *Primordial Nucleosynthesis in the Precision Cosmology Era*, *Annu. Rev. Nucl. Part. Sci.* **57** (2007) pg. 463.

[99] A. Ayala, I. Domínguez, M. Giannotti, A. Mirizzi, and O. Straniero, *Revisiting the Bound on Axion-Photon Coupling from Globular Clusters*, *Phys. Rev. Lett.* **113** (2014) pg. 191302.

[100] L. Piersanti, O. Straniero, and S. Cristallo, *A method to derive the absolute composition of the Sun, the solar system, and the stars*, *Astron. Astrophys.* **462** (2007) pg. 1051.

[101] A. M. Serenelli and S. Basu, *Determining the Initial Helium Abundance of the Sun*, *Astrophys. J.* **719** (2010) pg. 865.

[102] C. Pitrou, A. Coc, J. -P. Uzan, and E. Vangioni, *Precision big bang nucleosynthesis with improved Helium-4 predictions*, *Phys. Rep.* **04** (2018) pg. 005.

[103] M. Tasumi and A. Sakamoto eds., *Introduction to Experimental Infrared Spectroscopy*, Wiley, New York, NY (2015).